

Experimental study along the magnesio-hornblende–glaucophane join

JIE LEI^{1,2}, DAVID M. JENKINS^{1,*} AND KIYOTAKA ISHIDA³

¹Department of Geological Sciences and Environmental Studies, Binghamton University, Binghamton, New York 13902-6000, U.S.A.

²China Shenhua Overseas Development and Investment Company, Beijing 100025, China

³Department of Environmental Changes, Graduate School of Social and Cultural Studies, Kyushu University, 744 Motooka, Nishi-ku, Fukuoka 819-0395, Japan

ABSTRACT

Amphiboles have played a leading role in metamorphic petrology, from helping to define several metamorphic facies to forming the basis of geothermobarometry, if their thermodynamic mixing properties can be calibrated to the temperature and pressure of formation. Compositional variations of sodium- and sodium-calcium-amphiboles may reveal important information about paleo-subduction zones but have not been studied as much as the more common calcium-amphiboles. In this study we investigate the mixing properties of amphibole solid solutions between magnesio-hornblende and glaucophane [${}^{\text{B}}\text{Ca}_2(\text{Mg}_4\text{Al})^{\text{T}}(\text{AlSi}_7)\text{O}_{22}(\text{OH})_2$ – ${}^{\text{B}}\text{Na}_2(\text{Mg}_3\text{Al}_2)^{\text{T}}(\text{Si}_8)\text{O}_{22}(\text{OH})_2$] as a binary sub-join within the ternary amphibole system tremolite–glaucophane–tschermakite where the principal substitutions are Ca for Na at the B, Al for Mg at the C, and Al for Si at the T crystallographic sites. Amphiboles were made from mixtures of reagent oxides at 10 mol% increments between magnesio-hornblende and glaucophane, formed in a piston-cylinder press at 735–860 °C and 1.3–2.5 GPa for 72–216 h giving good yields (92–100 wt%). A positive deviation is present in the volume-composition plot, even after correcting volumes for non-binary components, supporting the presence of a positive deviation in the enthalpy of mixing (ΔH^{mix}) along this join. Fourier transform infrared spectra (FTIR) were obtained in the range of 350–4000 cm^{-1} for the mid-infrared spectra (MIR) for the purpose of estimating the extent of short-range ordering and for autocorrelation analysis, and, in the 650–50 cm^{-1} , for far-infrared spectra (FIR) for autocorrelation analysis. Autocorrelation analysis gave $\delta\Delta\text{Corr}$ values, which further support a positive deviation in the ΔH^{mix} along the magnesio-hornblende–glaucophane join, although the $\delta\Delta\text{Corr}$ maximum did not occur at the calcium-poor (i.e., glaucophane-rich) portion of the join as expected. Synthetic end-member glaucophane and magnesio-hornblende were mixed in a molar ratio of 1:1 and allowed to equilibrate by homogenization for variable durations in the range of 600–800 °C at 2.0 GPa to determine the maximum-width of the miscibility gap. These compositional re-equilibration experiments suggested the presence of an asymmetric miscibility gap (steeper toward glaucophane) with a critical-point below 700 °C. Combining the results of this study with previously published results on the tremolite–glaucophane join allowed refinement of several asymmetric formalism mixing parameters (i.e., $W_{\text{Gl,Ts}} = 20$ kJ, $\alpha_{\text{Ts}} = 1.2$) and modeling of the miscibility gap within the tremolite–glaucophane–tschermakite ternary system. The results showed that the composition of the critical point is very close to the maximum in the autocorrelation parameter $\delta\Delta\text{Corr}$, as one would predict. An important implication of this study is that low-temperature immiscibility between calcium- and sodium-rich amphiboles may be more important than the role of pressure, as proposed by Brown (1977), in accounting for the change in B-site Na contents of metamorphic amphiboles.

Keywords: Magnesio-hornblende, glaucophane, miscibility-gap, autocorrelation, infrared spectra, thermodynamic modeling

INTRODUCTION

Amphiboles are major rock-forming minerals in many metamorphic rocks, helping to define up to seven metamorphic facies (Liou et al. 1985; Vernon and Clarke 2008, p. 33). Their wide range of compositions offer considerable potential for deducing the pressures (P) and temperatures (T) under which a particular rock formed, as indicated by geothermobarometers that are in common use for calcium-amphiboles (e.g., Hammarstrom and

Zen 1986; Schmidt 1992; Holland and Blundy 1994). Rocks rich in glaucophane [${}^{\text{A}}\square{}^{\text{B}}\text{Na}_2(\text{Mg}_3\text{Al}_2)^{\text{T}}\text{Si}_8\text{O}_{22}(\text{OH})_2 = \text{Gl}$, where \square represents a vacancy] typically occur in blueschist-facies metamorphic terranes (e.g., Ernst 1963; Maruyama et al. 1996) so that any P - T information extracted from these amphiboles will help define the burial depths and/or geothermal gradients of the plate-convergent zones in which these rocks occur. Geothermobarometry involving sodium- or sodium-calcium-amphiboles has not been so extensively developed because of the difficulties of working experimentally with chemically complex natural amphiboles at low temperatures (Maruyama et al. 1986)

* E-mail: dmjenks@binghamton.edu

and because of the experimental challenges of working with end-member glaucophane at high temperatures (e.g., Jenkins and Corona 2006a). Recent advances in the synthesis of nearly end-member glaucophane (Jenkins and Corona 2006a) have provided opportunities for exploring basic questions about the energetics of cation mixing in sodium-rich amphiboles and, in turn, for calculating how their compositions vary with P and T .

In the survey of metamorphic amphiboles presented by Schumacher (2007), the compositions of most calcium-, sodium-calcium-, and sodium-amphiboles are comprised by the end-member compositions tremolite [${}^A\Box^B\text{Ca}_2\text{C}^C\text{Mg}_5\text{T}^T\text{Si}_8\text{O}_{22}(\text{OH})_2$, Tr], edenite [${}^A\text{Na}^B\text{Ca}_2\text{C}^C\text{Mg}_5\text{T}^T(\text{AlSi}_7)\text{O}_{22}(\text{OH})_2$, Ed], tschermakite [${}^A\Box^B\text{Ca}_2\text{C}^C(\text{Mg}_3\text{Al})^T(\text{Al}_2\text{Si}_6)\text{O}_{22}(\text{OH})_2$, Ts], and glaucophane. The edenite component is fairly minor in sodium-amphiboles as well as in coexisting sodium- and calcium-amphiboles, allowing us to model closely these amphibole compositions with the ternary system tremolite, glaucophane, and tschermakite. Considerable information is available on the stability and crystal-chemistry of tremolite (Jenkins 1987; Jenkins and Clare 1990; Welch and Pawley 1991; Maresch et al. 1994; Zimmermann et al. 1996; Gottschalk et al. 1999; Evans et al. 2000; Bozhilov et al. 2007) such that the conditions needed to make synthetic tremolite, even if not of ideal stoichiometry, are well established. Tschermakite is an important component in many amphibole-based exchange reactions; unfortunately, end-member tschermakite has not been synthesized (Jasmund and Schäfer 1972; Jenkins 1988, 1994; Cho and Ernst 1991; Hoschek 1995; Najorka and Gottschalk 2003). Instead, the limit of Al solid solution appears to be close to that of magnesio-hornblende [${}^A\Box^B\text{Ca}_2\text{C}^C(\text{Mg}_4\text{Al})^T(\text{AlSi}_7)\text{O}_{22}(\text{OH})_2$, Hb], a composition that lies halfway between tremolite and tschermakite. Finally, nearly pure glaucophane has been synthesized by Jenkins and Corona (2006a), Corona and Jenkins (2007), Jenkins (2011), Basora et al. (2012), and Corona et al. (2013) if strict control is maintained on the water content to prevent the formation of an expandable phyllosilicate (tri-octahedral smectite) and to limit the loss of soluble constituents (e.g., Na, Al, and Si) to the ambient fluid. Progress over the last two decades on the synthesis of tremolite, magnesio-hornblende, and glaucophane allows us to investigate the crystal-chemistry and energetics of cation mixing along several key compositional joins, namely, the tremolite–glaucophane join, which was recently studied by Jenkins et al. (2013, 2014), and the magnesio-hornblende–glaucophane join, the subject of this study. Together these two compositional joins provide fairly complete coverage of the compositional space relevant to sodium- and sodium-calcium amphiboles.

Synthesis of magnesio-hornblende of ideal composition has proven difficult. As with other calcium-amphiboles, there is a small but persistent tendency to have less than the theoretical value of 2 Ca and 2 Al atoms per formula unit (apfu), which has been discussed in more detail by Cao et al. (1986), Jenkins (1988, 1994), and Najorka and Gottschalk (2003). Therefore we used a magnesio-hornblende-rich amphibole with the nominal bulk composition ${}^A\Box^B(\text{Ca}_{1.85}\text{Mg}_{0.15})^C(\text{Mg}_{4.1}\text{Al}_{0.9})^T(\text{Si}_{7.1}\text{Al}_{0.9})\text{O}_{22}(\text{OH})_2$, named “A”. The slight depletion in Ca and Al and enrichment in Mg was chosen because of its likelihood of yielding essentially pure amphibole. Accordingly, experiments were

conducted strictly along the “A”–Gl join, slightly displaced from the Hb–Gl join, to maximize amphibole yields. We stress that data extracted from the amphiboles formed in this study is based on the observed, rather than presumed or nominal compositions, to account for any compositional deviations from the intended join.

Previous studies of metamorphic amphibole (e.g., Himmelberg and Papike 1969; Ernst 1979; Maresch et al. 1982; Reynard and Ballèvre 1988; Smelik and Veblen 1992) have documented that glaucophane shares a miscibility gap or solvus, rather than having complete solid solution, with calcic amphiboles. Accordingly, a primary focus of this study is to document the location of any miscibility gap along the Hb–Gl join. One indication of the presence of a miscibility gap can be seen in the volume-composition relationships along the Hb–Gl join, where the presence of a positive deviation from ideal mixing of molar volumes supports the tendency for unmixing. We also studied amphibole dissolution or re-equilibration of two end-member amphiboles mixed in a molar ratio of 1:1 to determine the location of the critical temperature and to place constraints on the maximum size of the miscibility gap.

There has been significant effort given to analyzing the infrared (IR) spectra of synthetic amphiboles in the past several decades, primarily in the OH-stretching region of 3800–3200 cm^{-1} for the purpose of deducing short-range order (e.g., Hawthorne et al. 2000; Hawthorne and Della Ventura 2007). More recently, analysis of mineral IR spectra in the mid- and far-IR range (1200–100 cm^{-1}) using the method known as autocorrelation has provided a means for characterizing the amount of interatomic strain and, therefore, the energetics associated with cation substitution within minerals (Salje et al. 2000). It is possible to use IR spectra to analyze mixing properties because the phonon spectra samples a length scale of several unit cells that contains much information about local strain associated with atomic substitutions in the lattice (Boffa Ballaran et al. 1998, 1999; Atkinson et al. 1999; Carpenter and Boffa Ballaran 2001; Tarantino et al. 2002; Carpenter 2002). Cation mixing and order/disorder within the amphibole structure can be detected by both IR peak shifts and band-width variations with changes in amphibole composition (Boffa Ballaran et al. 2001; Boffa Ballaran and Carpenter 2003). Autocorrelation is a convenient means of characterizing IR spectra that may be both complex and asymmetric in nature, using the Gaussian-based peak-width parameter ΔCorr , and the relative changes in this parameter expressed as $\delta\Delta\text{Corr}$, to reveal systematic changes in band width (Salje et al. 2000). Substitutions along a solid solution join with a positive excess volume and positive elastic energy typically leads to line-broadening, which, in turn, is correlated with the enthalpy of mixing (Boffa Ballaran and Carpenter 2003; Etzel and Benisek 2008). Even if absolute values for the enthalpy of mixing cannot be derived, Jenkins et al. (2014) proposed that autocorrelation analysis should at least provide the sense of asymmetry of the enthalpy or excess Gibbs free energy of mixing along the join. Therefore, we use infrared spectra in the OH-stretching region, mid-infrared, and far-infrared range of amphiboles formed in this study to gain additional insights into the short-range order and energetics of mixing along the Hb–Gl join.

METHOD

Amphibole synthesis and apparatus

All amphiboles were synthesized from mixtures of reagent grade oxides and carbonates (Na_2CO_3 , CaCO_3 , MgO , Al_2O_3 , and SiO_2). The SiO_2 was made from silicic acid heated in steps to 1100 °C in air, yielding amorphous silica or weakly crystalline cristobalite. After weighing and mixing the reagents Na_2CO_3 , CaCO_3 , Al_2O_3 , and SiO_2 , they were heated at 900 °C for 15 min to remove CO_2 . Magnesium was then added as $\text{Mg}(\text{OH})_2$ for most of the mixtures, using the hydroxide as the source of water. Only for one mixture (MgHG-1) was the $\text{Mg}(\text{OH})_2$ mixed in before decarbonation, to which 3 wt% of distilled water was added later. The bulk compositions of all samples investigated in this study are presented in Table 1.

Starting mixtures were treated in sealed Pt capsules, which were made from tubing that was cleaned in acetone and then oven- or flame-annealed to around 1200 °C. Pt capsules were either 4.0 mm outer diameter (OD) by 15 mm length (synthesis experiments) or 1.5 mm OD by 5.5 mm length (retreatment experiments) having wall thicknesses of 0.13–0.18 mm. A 1/2-inch diameter piston-cylinder press was used for all experiments with NaCl serving as the pressure medium and fitted with a straight graphite furnace. Temperatures were measured with a chromel–alumel thermocouple situated in the salt pressure media directly above the sample. The specific synthesis conditions are listed in Table 2.

Analytical equipment and methods

Powder X-ray diffraction analysis was done by grinding the samples in an agate mortar under ethanol. The powder was mounted on a zero background oriented quartz plate and analyzed by a Philips X'Pert PW3040-MPD diffractometer operated at 40 kV and 20 mA using $\text{CuK}\alpha$ radiation fitted with a diffracted-beam graphite monochromator. All of the samples were first analyzed from 5 to 50° 2 θ (short scan) with step sizes of 0.02° 2 θ to see whether the sample needed a retreatment or showed no additional amphibole growth. Once the samples were confirmed to have reached their optimal yield, a step scan over the range 8 to 100° 2 θ (long scan) at increments of 0.05° 2 θ was done for sufficient time (2–3 s/step) to obtain ~1000–2000 counts on the major peaks. Rietveld refinements were done using the program GSAS (Larson and Von Dreele 2000). Reagent grade NaCl (a_0

= 5.6401 Å) was added in the samples to serve as an internal standard to adjust the zero point of the patterns. Refinements were initiated using the structure of glaucophane from Papike and Clark (1968), pargasite (for hornblende) from Sharma and Jenkins (1999), talc from Perdrikatsis and Burzlaff (1981), quartz from Levien et al. (1980), and smectite using the vermiculite structure of Shirozu and Bailey (1966). The following parameters were adjusted during refinements of the long scans in the sequence indicated: (1) zero point relative to NaCl, but held constant there after; (2) background (Function 1, shifted Chebyshev); (3) scale factors; (4) unit-cell dimensions; (5) March-Dollase preferred orientation parameters; (6) terms LX and LY in the profile function (Function 2, pseudo-Voigt); (7) atomic coordinates; (8) site occupancies of Na and Ca at the $M(4)$ and of Na at the A site, and (9) isotropic displacement parameters (U_{iso}) if they could be stably refined. Site occupancies at the $T(1)$ and $M(2)$ sites were assumed to be fully occupied by Si and Al, respectively, because of the similarities in the scattering factors of Si, Al, and Mg. For short scans, refinements only involved the zero point, background, scale factors, March-Dollase preferred orientation, and cell dimensions, where the cell dimensions of the amphiboles are used to gauge the extent of compositional re-equilibration, as discussed below.

Electron microprobe (EMP) analysis was accomplished on a JEOL 8900 Superprobe. Samples were mounted in epoxy, polished with diamond grit in steps down to 0.5 μm , carbon coated, and analyzed under the conditions of 15 kV and 10 nA. The standards used were: diopside for Ca, albite for Na, and the pure oxides for Mg, Al, and Si.

We measured Fourier transform infrared spectra (FTIR) as mid-infrared spectra (MIR) and far-infrared spectra (FIR) at two different institutions. For the MIR spectra two sets of samples were prepared, one by embedding the sample in KBr pellets using a sample/KBr ratio of 0.7/200 mg for measurements in the lattice-vibration range (350–2000 cm^{-1}), the other using a sample/KBr ratio of 3/200 mg for measurements in the OH-stretching region (2000–4000 cm^{-1}). All pellets were prepared by compression in an evacuated die. MIR spectra were recorded in transmission mode with a Bruker Equinox 55 spectrometer at Binghamton University scanned 64 times at a resolution of 2.0 cm^{-1} under flowing nitrogen. The FIR spectra were obtained at Kyushu University, Japan, with a JASCO FTIR-620 spectrometer using either a Hg-lamp with 12 μm Mylar beam splitter or a globar source with 5 μm Mylar beam splitter. Two sets of spectra were recorded: (1) a small sample concentration of 0.8–1.1 mg and (2) a large sample concentration of 1.9–2.6 mg, both embedded in about 80 mg polyethylene disks 10 mm in diameter. These two concentrations were used in an attempt to improve the signal-to-noise ratio in different portions of the spectra. Samples were scanned 512 times at a resolution of 2 cm^{-1} , in the range of 650–50 cm^{-1} .

RESULTS

Amphibole yield

We synthesized individual amphiboles along the Hb–Gl join at conditions ranging from 760 °C/2.5 GPa (Gl-rich) to 860 °C/1.3 GPa (Hb-rich) for 72–216 h. In general, excellent amphibole yields (92–100%) were obtained. From Table 2, it is obvious that the Hb-rich amphiboles have a better yield than the Gl-rich counterparts, including even pure yields of amphibole,

TABLE 1. Bulk compositions of mixtures investigated in this study

Sample code prefix	Nominal bulk composition	Components ^a (mol%)
MgHG-10	$\text{Na}_2\text{Mg}_3\text{Al}_2\text{Si}_6\text{O}_{22}(\text{OH})_2$	$\text{Hb}_{0.0}\text{Cum}_{1.0}\text{Tr}_{0.0}\text{Gl}_{1.0}$
MgHG-9	$\text{Na}_{1.8}\text{Ca}_{0.185}\text{Mg}_{3.125}\text{Al}_{1.98}\text{Si}_{7.91}\text{O}_{22}(\text{OH})_2$	$\text{Hb}_{0.9}\text{Cum}_{0.75}\text{Tr}_{0.25}\text{Gl}_{0.9}$
MgHG-5	$\text{Na}_{1.6}\text{Ca}_{0.37}\text{Mg}_{3.25}\text{Al}_{1.96}\text{Si}_{7.82}\text{O}_{22}(\text{OH})_2$	$\text{Hb}_{1.6}\text{Cum}_{1.5}\text{Tr}_{0.5}\text{Gl}_{1.6}$
MgHG-3	$\text{Na}_{1.4}\text{Ca}_{0.555}\text{Mg}_{3.375}\text{Al}_{1.94}\text{Si}_{7.73}\text{O}_{22}(\text{OH})_2$	$\text{Hb}_{2.7}\text{Cum}_{2.25}\text{Tr}_{0.75}\text{Gl}_{2.7}$
MgHG-7	$\text{Na}_{1.2}\text{Ca}_{0.74}\text{Mg}_{3.5}\text{Al}_{1.92}\text{Si}_{7.64}\text{O}_{22}(\text{OH})_2$	$\text{Hb}_{3.6}\text{Cum}_{3.0}\text{Tr}_{1.0}\text{Gl}_{3.6}$
MgHG-1	$\text{Na}_{1.0}\text{Ca}_{0.925}\text{Mg}_{3.625}\text{Al}_{1.90}\text{Si}_{7.55}\text{O}_{22}(\text{OH})_2$	$\text{Hb}_{4.5}\text{Cum}_{3.75}\text{Tr}_{1.25}\text{Gl}_{4.5}$
MgHG-6	$\text{Na}_{0.8}\text{Ca}_{1.11}\text{Mg}_{3.75}\text{Al}_{1.88}\text{Si}_{7.46}\text{O}_{22}(\text{OH})_2$	$\text{Hb}_{5.4}\text{Cum}_{4.5}\text{Tr}_{1.5}\text{Gl}_{5.4}$
MgHG-2	$\text{Na}_{0.6}\text{Ca}_{1.295}\text{Mg}_{3.875}\text{Al}_{1.86}\text{Si}_{7.37}\text{O}_{22}(\text{OH})_2$	$\text{Hb}_{6.3}\text{Cum}_{5.25}\text{Tr}_{1.75}\text{Gl}_{6.3}$
MgHG-4	$\text{Na}_{0.4}\text{Ca}_{1.48}\text{Mg}_{4.0}\text{Al}_{1.84}\text{Si}_{7.28}\text{O}_{22}(\text{OH})_2$	$\text{Hb}_{7.2}\text{Cum}_{6.0}\text{Tr}_{2.0}\text{Gl}_{7.2}$
MgHG-8	$\text{Na}_{0.2}\text{Ca}_{1.665}\text{Mg}_{4.125}\text{Al}_{1.82}\text{Si}_{7.19}\text{O}_{22}(\text{OH})_2$	$\text{Hb}_{8.1}\text{Cum}_{6.75}\text{Tr}_{2.25}\text{Gl}_{8.1}$
MgHG-11 (= A)	$\text{Ca}_{1.85}\text{Mg}_{4.25}\text{Al}_{1.80}\text{Si}_{7.10}\text{O}_{22}(\text{OH})_2$	$\text{Hb}_{9.0}\text{Cum}_{7.5}\text{Tr}_{2.5}\text{Gl}_{9.0}$

^aComponent abbreviations and compositions: Hb (Hornblende) = $\text{Ca}_2(\text{Mg}_4\text{Al})(\text{AlSi}_7)\text{O}_{22}(\text{OH})_2$; Cum (Cummingtonite) = $\text{Mg}_2\text{Si}_6\text{O}_{22}(\text{OH})_2$; Tr (Tremolite) = $\text{Ca}_2\text{Mg}_5\text{Si}_8\text{O}_{22}(\text{OH})_2$; Gl (Glaucophane) = $\text{Na}_2(\text{Mg}_3\text{Al}_2)\text{Si}_6\text{O}_{22}(\text{OH})_2$.

TABLE 2. Treatment conditions and products of synthesis for mixtures investigated on the hornblende-glaucophane join

Sample code	Nominal Gl (mol%)	T (°C)	P (GPa)	t (h)	H_2O^c (wt%)	Products
MgHG-10-2.2 ^a	100	760(10)	2.50(3)	116.8	0	amph (99%), talc (1%)
MgHG-(R)9	90	755(20)	2.34(3)	72.0	0	amph (99.8%), smec (0.2%)
MgHG-(R)5-2.2 ^a	80	750(10)	2.25(3)	144.0	0	amph (99%), talc (1%)
MgHG-3.3 ^b	70	735(10)	1.8(3)	215.8	0	amph (92%), qtz (8%)
MgHG-(R)7-2.2 ^a	60	790(10)	2.12(3)	96.0	0	amph (95%), talc (4.5%), smec (0.5%), liq
MgHG-1.2 ^a	50	755(5)	2.00(3)	168.2	2.03	amph (97%), talc (3%)
MgHG-(R)6	40	805(20)	2.00(3)	72.0	0	amph (92%), talc (8%)
MgHG-2	30	760(10)	2.00(3)	71.3	0	amph (96%), talc (4%)
MgHG-(R)4-2	20	830(10)	1.50(3)	72.0	0	amph (100%)
MgHG-(R)8-2	10	830(10)	1.50(3)	72.0	0	amph (100%)
MgHG-11	0	860(20)	1.29(3)	72.0	0	amph (100%)

Notes: Uncertainties in last digit shown in parentheses. Proportions (wt%) of products are from the Rietveld refinements and involve only the crystalline phases. Abbreviations: amph = amphibole; qtz = quartz; smec = smectite; liq = quenched liquid or aqueous solute.

^aRetreatment of the previous synthesis, with intermediate grinding, at the same conditions. Time shown is the cumulative duration of both treatments.

^bThis sample was treated three separate times, with intermediate grinding. Time shown is the total duration of all treatments.

^c H_2O added to the starting mixture. For most experiments water is introduced as $\text{Mg}(\text{OH})_2$.

such as MgHG-(R)4-2, MgHG-(R)8-2 (Fig. 1a), and MgHG-11. Talc is the most common additional phase, though some of the extra phases can be removed during retreatment by increasing the reaction temperature. However, increasing the temperature may produce an amorphous phase, as seen for example by an elevated background in the XRD pattern of MgHG-(R)7-2.2 (Fig. 1b). This amorphous phase does not always coexist with talc, and in fact only appeared in MgHG-(R)7-2.2. It is not clear if it is a quenched silicate melt or a solute that precipitates from the ambient fluid upon quench. Besides talc and this amorphous material, quartz, and smectite also occur in the run products, but typically have an abundance below 10 wt%. Rarely pyroxene crystallized during the synthesis but generally could be eliminated with retreatment.

Amphibole compositions and textures

Amphibole compositions are listed in Table 3 and shown in Figures 2a and 2b. Projection of the synthesized amphibole compositions (open circles) from SiO₂ and H₂O into the Na₂O–CaO–MgO–Al₂O₃ tetrahedron in Figure 2a shows that the samples lie close to the intended join “A”–Gl (solid circles) and are closely modeled by the amphibole sub-tetrahedron Hb–Gl–Cm–Kt, where Cm is cummingtonite [^A□^BMg₂^CMg₃^TSi₈O₂₂(OH)₂] and Kt is katophorite [^ANa^B(NaCa)^C(Mg₄Al)^T(AlSi₇)O₂₂(OH)₂]. The latter component is included because deviation of sodium- and sodium-calcium-amphiboles toward enrichment in the katophorite component was noted in earlier studies (Graham et al. 1989; Pawley 1992; Jenkins et al. 2013). Compositional departures from the intended join are more apparent in Figure 2b, where the synthesized amphibole compositions (open circles) are projected from cummingtonite, quartz, and water onto the Gl–Tr–Ts ternary plane. This diagram demonstrates that small deviations from the intended join exist indicating some depletion in the Ts compo-

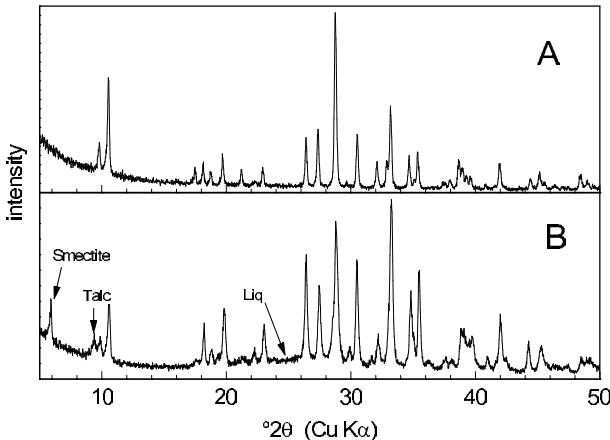


FIGURE 1. Powder XRD patterns of selected samples. (a) Powder XRD pattern obtained for Hb₈₁Mg_{6.75}Tr_{2.25}Gl₁₀ [MgHG-(R)8-2, Table 2] made at 830 °C, 1.5 GPa, for 72 h. The pattern shows essentially a pure yield of amphibole. (b) Powder XRD pattern obtained for Hb₃₆Mg₃Tr₁Gl₆₀ [MgHG-(R)7-2.2, Table 2] made at 790 °C, 2.12 GPa, for 96 h. The major peaks of non-amphibole phases (smectite, talc) are indicated, while the slightly elevated background in this pattern relative to that in a suggests a small proportion of amorphous material is present, labeled here as Liq.

nent near the middle of the join, but not significantly outside of the range of uncertainty for any given point as indicated by the representative error bars on Figure 2b. Overall, the agreement between the nominal and observed amphibole compositions is quite close as expected from the high synthesis yields.

Figure 3 presents representative backscattered electron (BSE) images of the amphiboles synthesized in this study. Figure 3a is from a sample that lies mid-way along this join (Gl₅₀). Crystals are bigger and more easily identified than at the Gl-rich end (Fig. 3b), where the grains occur as very fine-grained aggregates. Near the Hb-rich end of the join (Figs. 3c and 3d) the amphibole grains are distinctly larger.

TABLE 3. Compositions of amphiboles synthesized in this study, reported as the average of *n* analyses, given in wt%, cations per 23 O atoms, and cation site occupancies

Sample	MgHG-10-2.2 100 (Gl, mol%)	MgHG-(R)9 90	MgHG-(R)5-2.2 80	MgHG-3.3 70	MgHG-(R)7-2.2 60	
<i>n</i>	3	15	15	8	14	
wt%						
SiO ₂	46.9(17)	58.1(10)	50.3(41)	57.5(12)	55.1(14)	
Al ₂ O ₃	9.5(3)	13.4(6)	11.8(11)	13.1(4)	12.4(8)	
MgO	12.8(11)	16.2(11)	16.0(18)	18.9(9)	19.6(12)	
CaO	0.08(5)	1.6(3)	2.7(4)	4.3(5)	6.2(7)	
Na ₂ O	5.6(1)	7.8(5)	5.5(7)	5.8(3)	4.6(7)	
Total	75.0(28)	97.2(14)	86.3(77)	99.7(15)	97.9(9)	
Cations						
Si	7.97(2)	7.71(10)	7.54(8)	7.49(10)	7.35(12)	
Al	1.91(8)	2.10(9)	2.08(5)	2.01(4)	1.95(12)	
Mg	3.25(18)	3.20(20)	3.56(13)	3.67(17)	3.89(25)	
Ca	0.02(1)	0.23(4)	0.44(4)	0.60(7)	0.89(10)	
Na	1.84(7)	2.00(12)	1.61(10)	1.46(6)	1.18(17)	
Total	14.99(2)	15.24(12)	15.23(11)	15.24(11)	15.26(13)	
Site occupancies						
^T Si	7.97(2)	7.71(10)	7.54(8)	7.49(10)	7.35(12)	
^T Al	0.03(2)	0.29(10)	0.46(8)	0.51(10)	0.65(12)	
^C Al	1.88(9)	1.81(11)	1.62(8)	1.50(12)	1.30(15)	
^M Mg	3.12(9)	3.16(16)	3.38(8)	3.50(12)	3.69(17)	
^B Mg	0.13(9)	0.04(6)	0.18(6)	0.17(5)	0.20(10)	
^B Ca	0.02(1)	0.23(4)	0.44(4)	0.60(7)	0.89(10)	
^B Na	1.84(8)	1.73(7)	1.38(7)	1.23(11)	0.91(15)	
^A Na	0.00	0.28(12)	0.23(11)	0.24(11)	0.27(12)	
wt%						
Sample	MgHG-1.2	MgHG-(R)6	MgHG-2	MgHG-(R)4-2	MgHG-(R)8-2	MgHG-11
<i>n</i>	50	40	30	20	10	0
	10	15	10	18	16	23
wt%						
SiO ₂	51.8(16)	52.9(8)	53.8(17)	52.8(10)	49.1(32)	51.9(11)
Al ₂ O ₃	11.6(12)	12.3(5)	11.4(25)	11.1(11)	10.7(13)	11.6(7)
MgO	19.8(9)	20.1(4)	20.6(7)	21.6(9)	20.1(16)	21.1(6)
CaO	7.7(4)	9.2(3)	9.6(4)	11.0(6)	11.0(10)	12.1(9)
Na ₂ O	3.5(3)	2.9(2)	2.3(4)	1.3(2)	0.68(7)	0.02(2)
Total	94.4(31)	97.4(9)	97.7(13)	97.8(16)	91.6(61)	96.8(14)
Cations						
Si	7.21(7)	7.15(6)	7.24(22)	7.12(8)	7.08(10)	7.07(8)
Al	1.90(16)	1.96(8)	1.80(39)	1.77(17)	1.82(17)	1.86(12)
Mg	4.11(13)	4.04(9)	4.14(14)	4.35(16)	4.32(10)	4.28(11)
Ca	1.15(7)	1.33(4)	1.38(5)	1.58(8)	1.70(11)	1.77(14)
Na	0.94(8)	0.77(4)	0.60(10)	0.34(4)	0.19(2)	0.007(6)
Total	15.31(5)	15.25(5)	15.16(7)	15.17(7)	15.11(4)	14.99(4)
Site occupancies						
^T Si	7.21(7)	7.15(6)	7.24(22)	7.12(8)	7.08(10)	7.07(8)
^T Al	0.79(7)	0.85(6)	0.76(22)	0.88(8)	0.92(10)	0.92(8)
^C Al	1.11(12)	1.11(6)	1.04(17)	0.89(12)	0.90(9)	0.94(7)
^M Mg	3.89(12)	3.89(6)	3.96(17)	4.11(12)	4.10(9)	4.06(7)
^B Mg	0.22(4)	0.16(5)	0.18(7)	0.24(8)	0.21(11)	0.22(11)
^B Ca	1.15(8)	1.33(4)	1.38(5)	1.58(8)	1.70(11)	1.77(14)
^B Na	0.63(8)	0.52(4)	0.44(6)	0.17(7)	0.08(4)	0.005(5)
^A Na	0.31(5)	0.25(5)	0.16(7)	0.17(7)	0.11(4)	0.002(5)

Note: Uncertainties (1σ) in the last digit are given in parentheses.

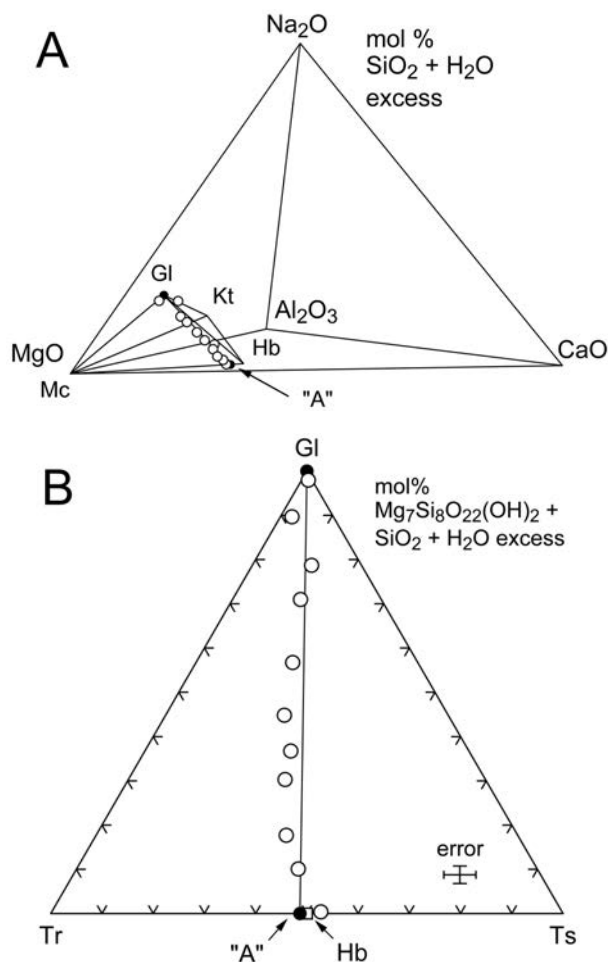


FIGURE 2. (a) Compositions of amphiboles synthesized in this study (open circles) at 10 mol% increments along the join “A”–Gl shown in the tetrahedron Na₂O–CaO–MgO–Al₂O₃ projected from SiO₂ and H₂O. The compositions of these samples are closely modeled by the amphibole tetrahedron magnesio-hornblende (Hb), cummingtonite (Cm), glaucophane (Gl), and katophorite (Kt). (b) Same amphibole compositions as shown in a but projected from Mg₇Si₈O₂₂(OH)₂ (cummingtonite), SiO₂, and H₂O onto the tshermakite (Ts)–tremolite (Tr)–Gl ternary plane. Representative error in the projected compositions is shown.

Unit-cell dimensions

Table 4 lists unit-cell dimensions for individual synthetic amphiboles determined from Rietveld refinements of the powder XRD patterns. Table 4 also includes selected whole-pattern agreement indices. Unit-cell dimensions are plotted in Figure 4a (open circles) as a function of Ca content (apfu). The curve fitted to the volume data is a polynomial regression, given in the figure, and includes the end-member volume for glaucophane (solid circle, 863 Å³) from the study of Jenkins and Corona (2006b). To gauge the effect of non-binary components on unit-cell volumes, the compositions of the amphiboles were recast into the components Gl, Hb, Cm, and Kt, which are given in Table 5, using the site-occupancy relations listed in the footnote to the table. Although this set of component is not unique, these components were chosen because they closely model the amphiboles formed in

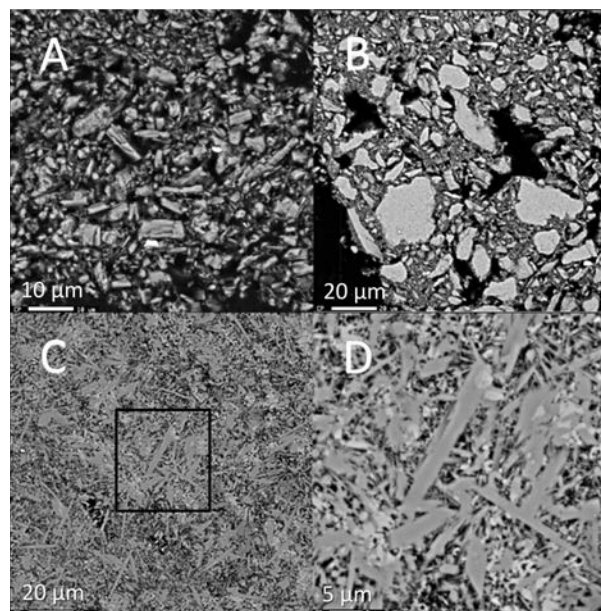


FIGURE 3. Backscattered electron images of representative samples of the amphiboles synthesized in this study. (a) Sample MgHG-1.2 (nominal Gl₅₀) treated at 755 °C and 2.0 GPa for 168 h. The amphibole (medium gray) constitutes about 97 wt% (Table 2) of this sample with talc (darker gray, matrix) being about 3 wt%. Amphibole occurs in a range of sizes with the largest grain at lower center being about 10 μm long and 3 μm wide. Scale is 10 μm. (b) Sample MgHG-10-2.2 (nominal Gl₁₀₀) treated at 760 °C and 2.5 GPa for 117 h. This sample shows the very fine-grained texture of pure glaucophane; the large bright areas are aggregates of fine grains. Scale is 20 μm. (c) Sample MgHG-11 (nominal Gl₀) treated at 860 °C and 1.3 GPa for 72 h. Pure “A” amphibole forms as numerous needles and elongate laths. Box is the area shown in d. Scale is 20 μm. (d) Enlargement of the central area of c showing the distinctly larger grain size of Hb-rich amphiboles, some reaching 25 μm long by 3 μm wide. Scale is 5 μm.

this study (Fig. 2a) and because the volumes of the components Cm and Kt are relatively well known, as noted below. Volumes were corrected back to the Hb–Gl join assuming a linear change in volume over relatively small changes in composition according to the relationship:

$$V_{\text{corr}} = [V_{\text{obs}} - (X_{\text{Cm}} \cdot V_{\text{Cm}} + X_{\text{Kt}} \cdot V_{\text{Kt}})] / (X_{\text{Gl}} + X_{\text{Hb}}) \quad (1)$$

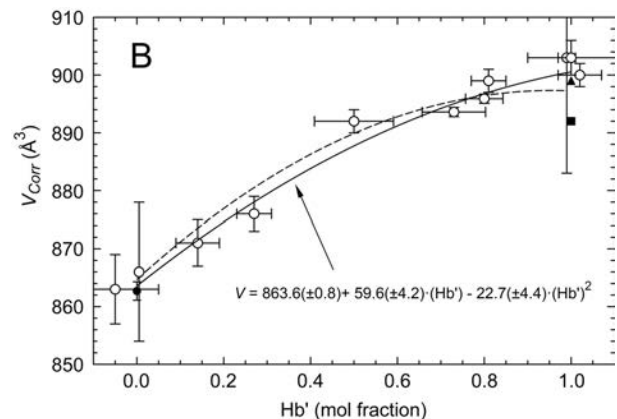
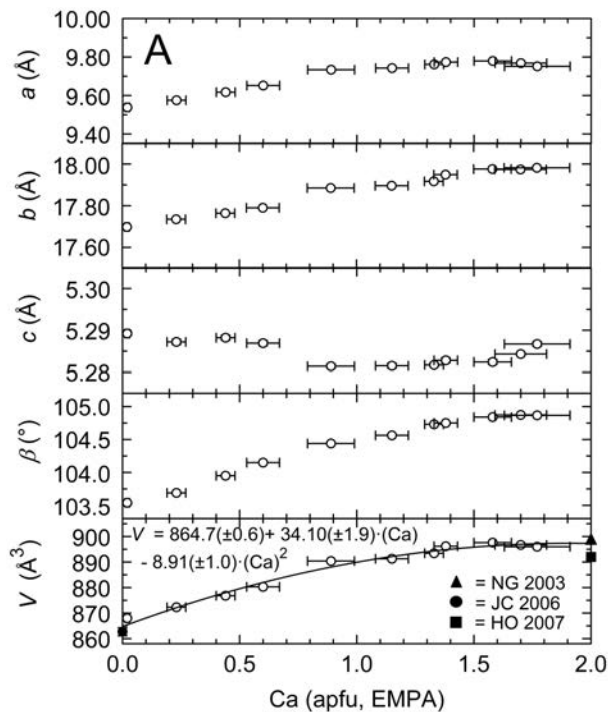
where V_{obs} is the observed volume, X_i is the mole fraction of component i , and V_i is the volume of pure component i . The unit-cell volumes adopted for this study are $V_{\text{Cm}} = 874.4 \text{ \AA}^3$ (extrapolated from heated $C2/m$ samples in the cummingtonite–grunerite join; Hirschmann et al. 1994) and $V_{\text{Kt}} = 893.1 \text{ \AA}^3$ (Jenkins et al. 2013).

Table 5 lists the calculated values of V_{corr} using Equation 1 and the mole fraction of the Hb component corrected for Cm and Kt, called Hb'. The corrected volumes are plotted against Hb' in Figure 4b. The solid curve is a polynomial (given in the figure) fit to the data but weighted by the inverse of the error in V_{corr} because of the large range (factor of 25) in the uncertainties of the corrected volumes. The dashed curve in Figure 4b is the polynomial fit to the original volume data from Figure 4a and is reported for comparison. As seen in Figure 4b, the volume correction causes only

TABLE 4. Unit-cell dimensions of synthetic amphibole made in this study and selected whole-pattern agreement indices

Sample code	Bulk Ca, apfu	<i>a</i> , Å	<i>b</i> , Å	<i>c</i> , Å	β , °	<i>V</i> , Å ³	GoF	DW- <i>d</i>	<i>R</i> _{wp}
MgHG-10-2.2	0.02(1)	9.5381(7)	17.698(2)	5.2892(4)	103.540(8)	868.0(1)	1.36	1.19	19.9
MgHG-(R)9	0.23(4)	9.5752(8)	17.735(2)	5.2872(6)	103.69(1)	872.3(1)	1.41	1.14	21.1
MgHG-(R)5-2.2	0.44(4)	9.6173(9)	17.764(2)	5.2882(6)	103.95(1)	876.8(1)	1.31	1.39	23.4
MgHG-3.3	0.60(7)	9.652(1)	17.790(2)	5.2869(6)	104.15(1)	880.3(1)	1.44	1.17	24.5
MgHG-(R)7-2.2	0.89(10)	9.734(1)	17.885(2)	5.2814(5)	104.44(1)	890.4(1)	1.35	1.33	19.4
MgHG-1.2	1.15(8)	9.7427(6)	17.896(2)	5.2815(6)	104.564(8)	891.3(1)	1.44	1.17	17.5
MgHG-(R)6	1.33(4)	9.7617(4)	17.917(1)	5.2817(4)	104.731(5)	893.45(7)	1.54	1.04	14.8
MgHG-2	1.38(5)	9.7736(6)	17.949(2)	5.2828(6)	104.751(7)	896.2(1)	1.35	1.26	21.9
MgHG-(R)4-2	1.58(8)	9.7793(6)	17.976(2)	5.2824(6)	104.841(7)	897.6(1)	1.25	1.57	22.4
MgHG-(R)8-2	1.70(11)	9.7681(4)	17.974(1)	5.2843(3)	104.874(5)	896.70(7)	1.68	0.94	16.2
MgHG-11	1.77(14)	9.7517(6)	17.982(2)	5.2867(5)	104.868(7)	896.0(1)	1.69	0.83	26.1

Notes: Uncertainties in the last digit (1 σ) given in parentheses. The whole-pattern refinement indices are: GoF is Goodness of Fit = $R_{wp}/R_{exp} = \sqrt{\chi^2}$; DW-*d* is the Durbin-Watson *d* statistic (Hill and Flack 1987), R_{wp} = weighted pattern agreement index (with background). The unit-cell parameters of *a*, *b*, *c*, β , and volume (*V*) were derived with halite as an internal standard.



▲▲ FIGURE 4. (a) Open circles are the unit-cell dimensions [*a*, *b*, *c*, (β), β (°), and *V* (Å³)] plotted as a function of the observed Ca contents (apfu) from electron microprobe analysis (EMPA, Table 3). Curve shown for the volumes is a second-order polynomial, indicated on the figure, fitted to the open circles and the volume for end-member glaucophane (solid circle) from Jenkins and Corona (2006). Shown for comparison are the volumes for magnesio-hornblende extrapolated from the data of Najorka and Gottschalk (2003, NG2003), and from the equations given by Hawthorne and Oberti (2007, HO2007). (b) Volumes corrected for the components Cm and Kt using Equation 1 as described in the text and projected onto the Hb-Gl join. Solid curve is a polynomial fit to the corrected volumes (*V*_{corr}) and weighted by the inverse of the uncertainty of each volume. Data are taken from Table 5. Dashed line is the same curve shown in **a** provided for comparison. Other symbols as in **a**.

a modest shift in the volume-composition relationships.

Two observations can be drawn from the relations given in Figure 4. First, the volume of end-member magnesio-hornblende ($Hb' = 1.0$) calculated from the polynomial given in Figure 4b gives a volume of 900.5 ± 3.0 Å³. This is in excellent agreement with the volume of end-member magnesio-hornblende derived from cell-dimension equations reported by Najorka and Gottschalk (2003, 899 Å³, solid triangle) based on their study of amphiboles formed along the tremolite-tschermakite join, but larger than the volume given by the equations in Hawthorne and Oberti (2007, 892 Å³, solid square) based on multiple regression analysis of the extensive IGG-CNR-PV amphibole database. It appears that the unit-cell volume of magnesio-hornblende based on experimental studies of chemically simplified systems are converging to a value of about 900 Å³; the reason for the discrepancy with the value

derived from the IGG-CNR-PV amphibole database is unknown at this time. Second, the volume data, whether corrected or not for non-binary components, show a clear positive deviation from an ideal (straight line) trend. This indicates an excess volume of mixing between the Hb and Gl components and is consistent with a positive enthalpy of mixing along this join (e.g., Davies and Navrotsky 1983) and the potential presence of a miscibility gap.

Glaucophane and amphibole “A” re-equilibration experiments

A second set of experiments were done to locate the miscibility gap along this join, or at least to provide constraints on the temperature of the critical point. Synthetic amphibole “A” and glaucophane were mixed in a molar ratio of 1:1 (MgHG-mixture) and treated at the conditions listed in Table 6 to determine if they would undergo

homogenization to either a single amphibole or to a mixture of two coexisting amphiboles. Using end-member compositions in these experiments means that incomplete re-equilibration would define only the maximum extent of the miscibility gap because the reaction rate becomes slower near the equilibrium phase boundary. The run products of these treatments are mainly one or two amphiboles with minor talc, smectite, and/or quartz (Table 6). We made no attempt to try and define the minimum width of the miscibility gap by exsolution of a single-phase amphibole into two amphiboles owing to the low temperatures involved (<700 °C) and the limited success of this approach for the closely related tremolite-glaucophane join reported by Jenkins et al. (2014).

Documenting changes in amphibole composition by electron microprobe analysis for these fine-grained amphiboles (Fig. 3) is difficult and gave highly scattered results for the tremolite-glaucophane join (Jenkins et al. 2014). Instead, we have employed the volume-composition relationship given in Figure 4a for amphiboles formed in this study, to determine their compositions. Although an indirect analytical method, it has the distinct advantage of providing the average composition of a large number of grains because the X-ray beam typically covers at least 50% of the sample area in the angular range (20–40 °2 θ) of maximum peak intensities. The volumes of single-phase or coexisting amphiboles were measured by XRD analysis, refined with the program GSAS, and are listed in Table 7. We note here that the Rietveld full-pattern method is well suited for dealing with mixtures of

phases of similar structure (e.g., feldspars) as discussed by Bish and Post (1993), so long as the reflections are sufficiently well resolved. Treatments at 800 and 750 °C readily re-equilibrated to a single, homogeneous amphibole; however, at 700 °C and lower the reaction rate was slower. Therefore, time-series experiments were implemented to provide some sense of the rate of compositional change. Figure 5 shows the change in amphibole composition with time for samples treated at 600, 650, and 700 °C. At 600 and 650 °C (Figs. 5a and 5b) we detected no statistically significant change in amphibole compositions and relative peak heights after 11 and 14 days, respectively, and further treatments were halted. However, at 700 °C (Fig. 5c) there was a noticeable change in compositions of the amphiboles after the first 10 days and treatments were continued until the two amphiboles gradually homogenized to a single amphibole after about 20 days. The XRD powder patterns for the 700 °C series are shown in Figure 6 (MgHG-M₂-series from Table 7), where some of the readily resolved peaks of glaucophane are indicated by arrows labeled with their Miller indices. The marked peaks show a tendency to either decrease in intensity or combine with the hornblende peaks and then gradually become sharper going from the bottom pattern (starting mixture) to the top (final treatment).

The results of the amphibole re-equilibration experiments are shown on the temperature-composition diagram in Figure 7. The small solid dots indicate the starting composition of the amphiboles, also determined using the volume-composition equation

TABLE 5. Compositions of amphiboles from Table 3 recast into the mole fractions of Gl, Hb, Cm, and Kt, the corrected composition Hb', and the corresponding corrected volume V_{corr}

Sample code	Amphibole components (mole fractions)					V_{obs} (Å ³)	V_{corr} (Å ³)
	Gl	Hb	Cm	Kt	Hb'		
MgHG-10-2.2	0.94(4)	0.005(4)	0.05(4)	0.001(3)	0.005(5)	868.0(1)	866(12)
MgHG-(R)9	0.72(8)	-0.02(5)	0.02(3)	0.28(12)	-0.05(10)	872.3(1)	863(6)
MgHG-(R)5-2.2	0.58(8)	0.10(5)	0.09(3)	0.23(11)	0.14(5)	876.8(1)	871(4)
MgHG-3.3	0.49(10)	0.18(4)	0.09(2)	0.24(11)	0.27(4)	880.3(1)	876(3)
MgHG-(R)7-2.2	0.32(10)	0.31(7)	0.10(5)	0.27(12)	0.50(9)	890.4(1)	892(2)
MgHG-1.2	0.16(6)	0.42(4)	0.11(2)	0.31(5)	0.73(7)	891.3(1)	893.6(8)
MgHG-(R)6	0.13(4)	0.54(3)	0.08(2)	0.25(5)	0.80(4)	893.45(7)	895.9(8)
MgHG-2	0.14(4)	0.61(5)	0.09(3)	0.16(7)	0.81(4)	896.2(1)	899(2)
MgHG-(R)4-2	0.00(6)	0.71(5)	0.12(4)	0.17(7)	1.00(10)	897.6(1)	903(3)
MgHG-(R)8-2	-0.01(4)	0.79(6)	0.11(6)	0.11(4)	1.02(5)	896.70(7)	900(2)
MgHG-11	0.002(4)	0.88(7)	0.11(6)	0.002(5)	0.99(2)	896.0(1)	903(20)

Notes: Mole fractions of the amphibole components were calculated from the analyses given in Table 3 as follows: Gl = ⁶Na-⁴Na/2, Hb = ⁶Ca-⁴Na/2, Cm = ⁶Mg/2, Kt = ⁴Na. Hb' is the mole fraction of Hb excluding Cm or Kt components. V_{obs} is the observed unit-cell volume (Table 4) while V_{corr} is the volume corrected back to the Hb-Gl join using Equation 1 in the text. Uncertainty in the last digit is shown in parentheses.

TABLE 6. Treatment conditions and re-equilibration products of coexisting glaucophane and magnesio-hornblende "A" mixed in a molar ratio of 1:1 and treated for different durations

Sample code	T (°C)	P (GPa)	t (h)	H ₂ O (wt%)	Products
MgHG-M ₃	600(5)	2.00(3)	143.6	3	Gl-amph, Hb-amph, talc
MgHG-M ₃ -2 ^a	600(5)	2.00(3)	258.9	3	Gl-amph, Hb-amph, talc, qtz(?)
MgHG-M ₅	650(5)	2.02(3)	166.5	3	Gl-amph, Hb-amph, smec, qtz
MgHG-M ₅ -2 ^a	650(5)	2.02(3)	338.5	3	Gl-amph, Hb-amph, qtz, talc
MgHG-M ₂	700(5)	2.00(5)	119	3	Gl-amph, Hb-amph, qtz
MgHG-M ₂ -2 ^a	700(5)	2.00(5)	238	3	Gl-amph, Hb-amph, qtz
MgHG-M ₂ -3 ^a	700(5)	2.00(5)	356.8	3	Gl-amph, Hb-amph, smec, qtz
MgHG-M ₂ -4 ^a	700(5)	2.00(5)	476.8	3	amph, qtz, smec
MgHG-M ₄	750(5)	2.07(3)	159.4	3	amph, talc
MgHG-M ₄ -2 ^a	750(5)	2.07(3)	201.3	3	amph, talc
MgHG-M ₁	800(5)	2.00(5)	71	3	amph

Notes: Uncertainties in last digit are shown in parentheses. Gl-amph = Gl-rich amphibole, Hb-amph = Hb-rich amphibole. Other abbreviations as in Table 2.
^a Retreatment of the previous treatment with intermediate grinding. Time shown is the cumulative duration.

TABLE 7. Amphibole volumes and corresponding compositions from the re-equilibration experiments reported in Table 6

Sample code	T (°C)	V		Composition (Ca, apfu)	
		Gl	Hb	Gl	Hb
MgHG-mixture	–	867.8(1)	894.5(1)	0.09(2)	1.36(13)
MgHG-M ₃ -1	600	870.66(2)	895.4(2)	0.18(3)	1.45(15)
MgHG-M ₃ -2 ^a	600	866.7(3)	892.2(3)	0.06(2)	1.16(11)
MgHG-M ₅ -1	650	869.65(3)	892.83(2)	0.15(3)	1.20(11)
MgHG-M ₅ -2 ^a	650	864.1(3)	891.8(3)	-0.02(2)	1.13(10)
MgHG-M ₂ -1	700	869.59(3)	891.6(2)	0.15(3)	1.11(10)
MgHG-M ₂ -2 ^a	700	884.24(3)	893.17(2)	0.70(7)	1.23(12)
MgHG-M ₂ -3 ^a	700	884.91(3)	891.6(3)	0.73(7)	1.12(10)
MgHG-M ₂ -4 ^a	700	884.0(3)	–	0.69(6)	–
MgHG-M ₄ -1	750	881.9(4)	892.5(6)	0.60(6)	1.18(11)
MgHG-M ₄ -2 ^a	750	–	888.3(2)	–	0.91(8)
MgHG-M ₁	800	–	883.4(2)	–	0.66(6)

Note: Uncertainties in last digit shown in parentheses.

^a Retreatment of the previous treatment with intermediate grinding. Time shown is the cumulative duration.

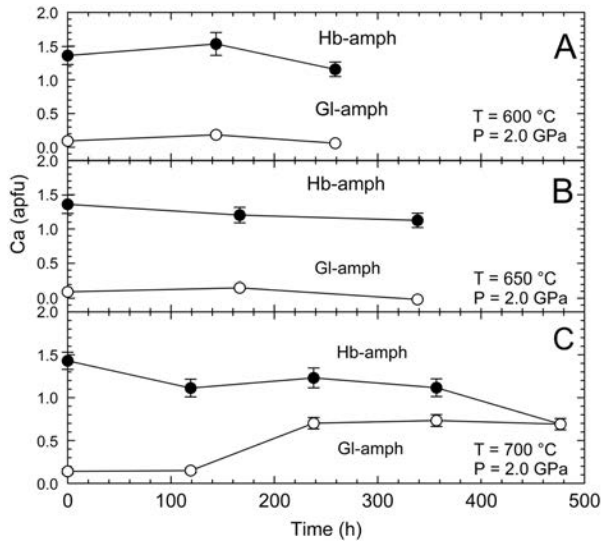


FIGURE 5. Amphibole re-equilibration experiments involving the dissolution of Hb-rich amphibole (solid circles) and Gl-rich amphibole (open circles) as a function of time. (a) Results at 600 °C and 2 GPa (MgHG-M3-series, Table 6). (b) Results at 650 °C and 2 GPa (MgHG-M5-series, Table 6). (c) Results at 700 °C and 2 GPa (MgHG-M2-series, Table 6). Note the convergence to a single amphibole at 700 °C.

of Figure 4a, whereas the open circles and squares indicate the compositions of re-equilibrated Gl- and Hb-rich amphiboles, respectively. The arrows show the sense of composition change. Note that the Gl-rich amphiboles at 600 and 650 °C show either very little change or even a small decrease in their Ca contents. Such minor Ca variations are probably within the analytical precision of this method; however, this is the strongest evidence that the Ca-poor side of the miscibility gap has a fairly steep limb whereas the Ca-rich side slopes more gently. Such behavior is observed in other joins where the steeper limb occurs near the end-member with the smaller cation as seen, for example, for the joins enstatite–dopside (Lindsley and Dixon 1976), halite–sylvite (Walker et al. 2005), and albite–orthoclase (Benisek et al. 2014). The miscibility gap shown in Figure 7 was calculated as discussed below.

Autocorrelation analysis of FTIR spectra

Spectra in the mid-infrared range (MIR) were recorded at 350–4000 cm^{-1} and lattice-vibration region, which is considered to be more sensitive to interatomic strain, is presented in Figure 8. We consider interference from non-amphibole phases in the lattice vibration region to be negligible because of the high amphibole yields in this study (Table 2). In the region 800–700 cm^{-1} , the relatively sharp and well-defined absorption bands observed for the end-member spectra become broader bands for the intermediate compositions, consistent with the development of increased strain at the more highly mixed intermediate compositions (e.g., Carpenter 2002). In addition, a gradual shift in the band positions above 600 cm^{-1} to higher wavenumbers occurs with increasing Gl content (from bottom to top) indicating an increase in vibration frequencies with reduction in unit-cell volume. Far-infrared spectra (FIR) in the range of 100–350 cm^{-1} shown in Figure 9 exhibit a similar band broadening for inter-

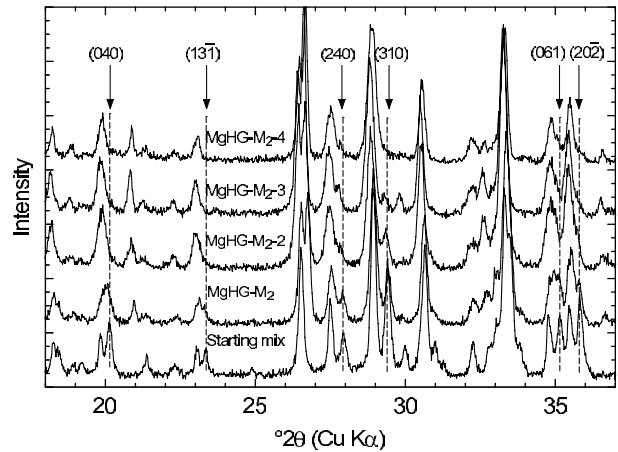


FIGURE 6. Powder XRD patterns showing the homogenization of glaucophane and amphibole “A” into a single amphibole in the time-series experiments done at 700 °C and 2 GPa for a total of 477 h (MgHG-M₂-series, Table 7). Vertical arrows and dashed lines indicate the location of several free-standing XRD peaks of glaucophane, labeled with the corresponding indices, in the starting mixture. By the last treatment (MgHG-M₂-4) there is essentially one amphibole present.

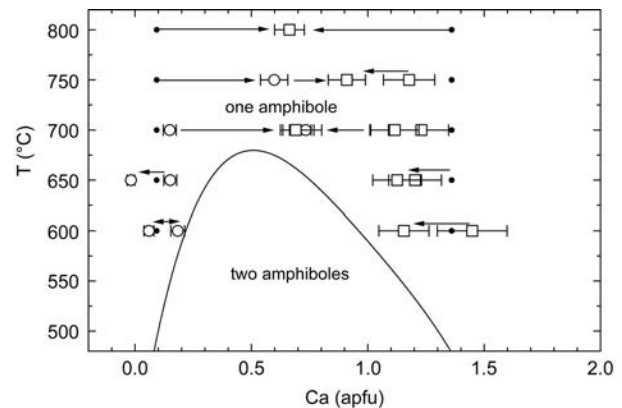


FIGURE 7. Temperature-composition diagram showing the amphibole re-equilibration results (Table 7). Small dots indicate the starting compositions of the amphiboles, the open circles are the compositions of Gl-rich amphiboles, and open squares are the compositions of Hb-rich amphiboles. Arrows indicate the sense of compositional re-equilibration. Miscibility gap separating the fields of one- and two-amphibole stability is a binary section through the ternary amphibole system Gl-Tr-Ts as discussed in the text. The solid curve shown here is represented by the following 4th-order polynomial: T (°C) = $370.70 + 1535.32 \times (\text{Ca, apfu}) - 2558.81 \times (\text{Ca}^2) + 1653.95 \times (\text{Ca}^3) - 411.53 \times (\text{Ca}^4)$.

mediate compositions but no consistent shift in band frequencies with change in composition.

Autocorrelation analysis has been applied to four wavenumber ranges, namely, (1) 162–224 cm^{-1} (= 200 cm^{-1}), (2) 328–407 cm^{-1} (= 360 cm^{-1}), (3) 410–610 cm^{-1} (= 500 cm^{-1}), and (4) 620–1300 cm^{-1} (= 800 cm^{-1}). The observed changes in band widths, expressed by the parameter ΔCorr (cm^{-1}), are plotted as a function of composition in Figure 10. Only the results for the 200 and 800 cm^{-1} ranges yielded systematic variations in ΔCorr ,

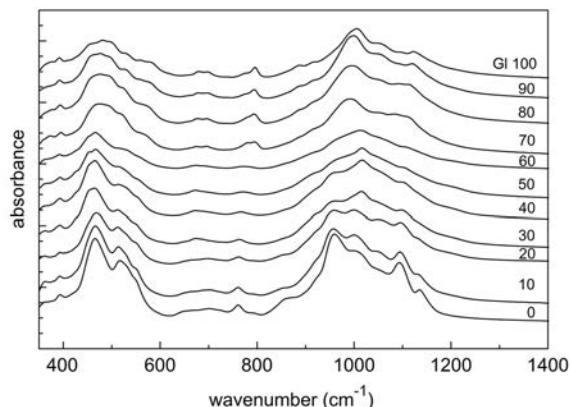


FIGURE 8. Infrared spectra in the MIR range of the amphiboles formed in this study, labeled with the nominal mol% of the Gl component.

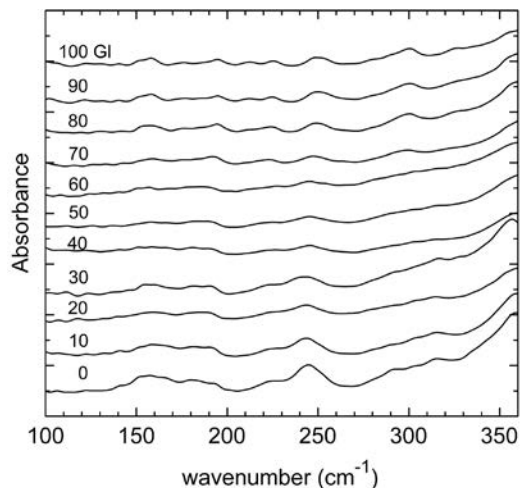


FIGURE 9. Infrared spectra in the FIR range of the amphiboles formed in this study, labeled with the nominal mol% of the Gl component.

whereas the 360 and 500 cm^{-1} ranges yielded highly scattered values. Figure 11 shows the same data but expressed as $\delta\Delta\text{Corr}$, namely the difference between ΔCorr and the straight baseline between the end-members of the join as illustrated in Figure 10d. The $\delta\Delta\text{Corr}$, or relative band-width changes, have been correlated with enthalpy of mixing (Boffa Ballaran and Carpenter 2003; Etzel and Benisek 2008). Even if absolute values of the enthalpy of mixing (ΔH^{mix}) cannot yet be reliably derived from the autocorrelation data, it was argued by Jenkins et al. (2014) that the positive deviation from ideal mixing and the sense of asymmetry in the mixing along a compositional join should be revealed by the autocorrelation results. Results from the 360 and 500 cm^{-1} ranges are too scattered to be useful; however, a two-parameter asymmetric Margules formulation (e.g., Davies and Navrotsky 1983) was used to model the $\delta\Delta\text{Corr}_{200}$ and $\delta\Delta\text{Corr}_{800}$ data in Figures 11a and 11d. The excess Gibbs free energy of mixing can be approximated by the enthalpy of mixing and therefore $\delta\Delta\text{Corr}$ as follows:

$$\Delta G^{\text{Excess}} \approx \Delta H^{\text{mix}} \propto \delta\Delta\text{Corr} = (W_{\text{Gl}}X_{\text{Hb}} + W_{\text{Hb}}X_{\text{Gl}})X_{\text{Gl}}X_{\text{Hb}} \quad (2)$$

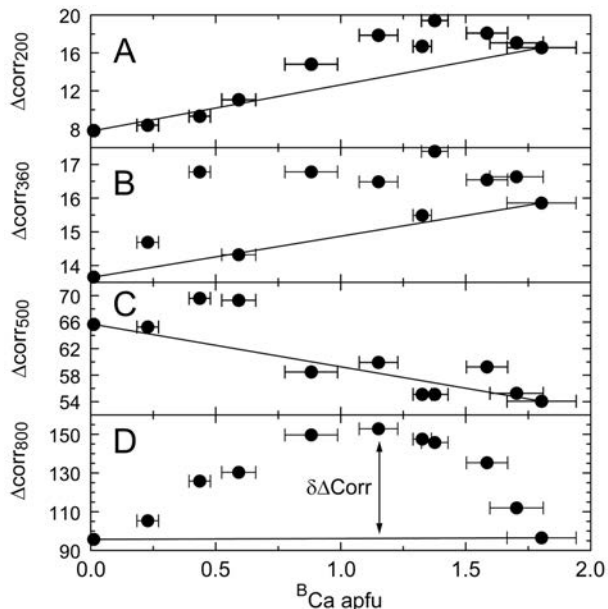


FIGURE 10. Plot of the autocorrelation band-width parameter ΔCorr , vs. the observed Ca cations (apfu) for four regions of the MIR spectra: (a) 162–224 cm^{-1} (= 200 cm^{-1}), (b) 328–407 cm^{-1} (= 360 cm^{-1}), (c) 410–610 cm^{-1} (= 500 cm^{-1}), and (d) 620–1300 cm^{-1} (= 800 cm^{-1}).

where X_i is the mole fraction of end-member i and W_i is the corresponding interaction parameter. Equation 2 was used to fit the $\delta\Delta\text{Corr}_{200}$ and $\delta\Delta\text{Corr}_{800}$ data with the resulting interaction parameters, in units of wavenumbers, indicated on Figures 11a and 11d, respectively. Although there is clearly a positive deviation from ideal mixing of the end-members, the surprising result is that the sense of asymmetry in the mixing energetics is the opposite of what is expected, with the data skewed toward the larger-volume rather than the smaller-volume Gl-rich portion of the join. A similar situation was encountered for the Ca-Tschermak–diopside join by Etzel and Benisek (2008), where the skew of the $\delta\Delta\text{Corr}$ data was opposite to the calorimetrically measured ΔH^{mix} . A resolution to these apparently contradictory results between the dissolution experiments and autocorrelation analysis will be offered below.

Short-range ordering

Because OH-stretching bands in amphibole are sensitive to the local atomic environment, important additional information about the octahedral, tetrahedral, and A-site cation occupancy near the OH group can be determined (e.g., Della Ventura et al. 1999; Hawthorne et al. 2000). Therefore, a second set of MIR spectra were measured with an increased sample/KBr ratio of 3/200 mg to enhance the intensity in the OH-stretching region. Essentially all of the spectra had broad bands centered at about 3500 cm^{-1} attributed to moisture absorbed by the sample. Spectra that could be adequately modeled with symmetric pseudo-Voigt profiles and from which band positions and relative intensities were extracted are listed in Table 8. Several spectra are shown in Figure 12, where the dots are the observed and the solid curve the modeled spectrum.

The configuration notation used throughout the following

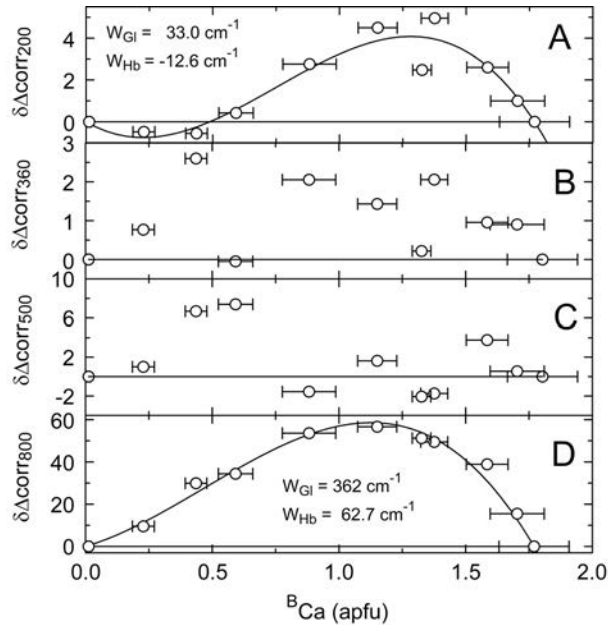


FIGURE 11. Values of $\delta\Delta_{\text{corr}}$ derived from the data in Figure 10 plotted against the observed Ca (apfu). The data in **a** and **d** were fitted to an asymmetric two-parameter expression similar to that used to model enthalpy of mixing and the derived parameters are listed on the plot. The data in **b** and **c** are too scattered to permit any simple fit.

TABLE 8. Modeled component band positions (cm^{-1}) and relative intensities in the OH-stretching region

Sample code	Nom. Gl (mol%)	Band position and relative intensities					
		A'	A	B	B'	C	D
MgHG-10-2.2	Gl ₁₀₀	–	–	3664 0.583	3673 0.417	–	–
MgHG-(R)9	Gl ₉₀	3638 0.156	3653(?) 0.008	3664 0.798	–	3681 0.038	–
MgHG-(R)5-2.2	Gl ₈₀	3640 0.059	–	3665 0.762	–	3686 0.006	3724 0.173
MgHG-3.2	Gl ₇₀	3646 0.128	3654 0.010	3665 0.571	–	3685 0.037	3713 0.254
MgHG-1.2	Gl ₅₀	–	3655 0.438	3676 0.351	–	3692 0.046	3713 0.165
MgHG-2	Gl ₃₀	–	3658 0.581	3673 0.312	–	3700 0.039	3714 0.068
MgHG-(R)4-2	Gl ₂₀	–	3655 0.467	3672 0.409	–	3693 0.020	3709 0.104
MgHG-(R)8-2	Gl ₁₀	–	3651 0.465	3670 0.505	–	3686 0.018	3742 0.013

discussion was introduced by Della Ventura et al. (1999) and Hawthorne et al. (2000). End-member glaucophane (MgHG-10-2.2, Fig. 12), with essentially no $^{\text{T}}\text{Al}$ and no $^{\text{A}}\text{Na}$ (Table 3), has only one readily identifiable asymmetric band, similar to the Gl-rich spectra reported earlier by Palin et al. (2003) and Jenkins and Corona (2006a). We chose to model this with two bands, the dominant band (B) at 3664 cm^{-1} and a smaller shoulder band (B') at 3674 cm^{-1} . The B band occurs in all of the samples in the range $3664\text{--}3674\text{ cm}^{-1}$ and is assigned to the $\text{MgMgMg}\text{--}\square\text{--SiSi}$ configuration for the $M(1)M(1)M(3)\text{--}A\text{--}T(1)T(1)$ sites (e.g., Della Ventura et al. 2003). This band shifts from 3670 cm^{-1} for Hb-rich to 3664 cm^{-1} for Gl-rich amphiboles, which is consistent with the small shift to lower frequencies with substitution

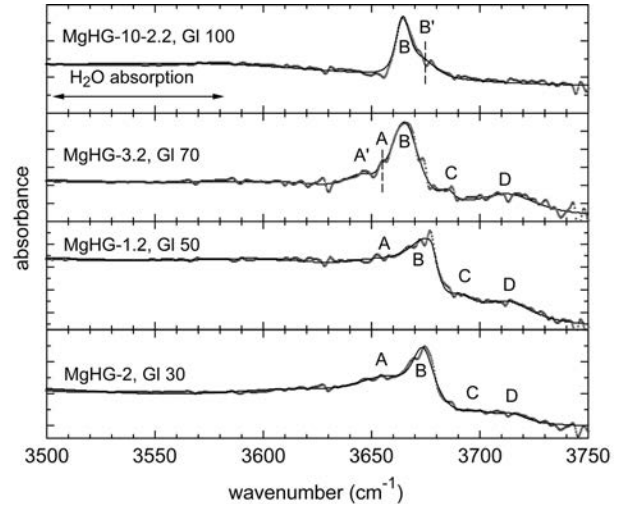


FIGURE 12. Infrared spectra in the OH-stretching region of selected synthetic amphiboles from this study labeled with the sample codes and nominal mol% Gl component. The observed intensities are represented by dots while the modeled intensities are shown by a solid curve. The broad absorption band centered near 3500 cm^{-1} is attributed to moisture absorbed by the sample. Locations of main band components are shown by letters.

of Na at the $M(4)$ and Al at the $M(2)$ sites, both fairly distant from the O(3) site, in glaucophane as observed by Jenkins et al. (2013) and as observed for $M(4)$ site substitutions in richteritic amphiboles by Iezzi et al. (2010). The shoulder B' band in end-member glaucophane is also attributed to the $\text{MgMgMg}\text{--}\square\text{--SiSi}$ configuration, but having Mg rather than Na at the neighboring $M(4)$ sites, as proposed by Jenkins et al. (2013) and supported by the presence of $^{\text{B}}\text{Mg}$ in this sample (Table 3).

The remaining spectral features can be divided into two regions using band B as the center: one having lower frequencies (e.g., bands A and A') corresponding to substitutions at the octahedral and tetrahedral sites in A-site-vacant local configurations, and one at higher frequencies (e.g., bands C and D) corresponding to the region of A-site-filled local configurations. At lower frequencies, band A occurs in the range of $3651\text{--}3658\text{ cm}^{-1}$ for the Hb-rich samples. Interference from adjacent water absorption bands makes determination of the A band's relative intensity difficult, which may result in spuriously high values listed in Table 8. This band is assigned to the $\text{MgMgMg}\text{--}\square\text{--SiAl}$ configuration because of an overall increase in its intensity with increasing Hb component (Table 8) and because it has a frequency shift consistent with substitution of Al at the $T(1)$ site (Hawthorne et al. 2000). Substitution of Al at the more distant $M(2)$ site produces only a small inductive shift in the OH-vibration, but substitution of Al at the $M(1)$ or $M(3)$, typical of synthetic and more disordered amphiboles, should produce a noticeable shift to lower frequencies. The fairly low intensity band A' at $3644\text{--}3646\text{ cm}^{-1}$ for samples MgHG-(R)9, MgHG-(R)5-2.2, and MgHG-3.2 is assigned to the $\text{MgMgAl}\text{--}\square\text{--SiSi}$ configuration (Hawthorne et al. 2000; Della Ventura et al. 2003) because of the large frequency shift. The occurrence of this weak band in amphiboles with high $^{\text{C}}\text{Al}$ content (Table 8) suggests minor Al at the $M(3)$ site (Oberti et al. 1995). At higher fre-

quencies, band C at 3681–3700 cm^{-1} and band D at 3709–3742 cm^{-1} appear in samples containing appreciable $^{\text{A}}\text{Na}$ (Table 8); accordingly, these bands are assigned to the MgMgAl-Na-SiAl and MgMgMg-Na-SiSi configurations, respectively, proposed by Della Ventura et al. (1999, 2003). From these observations, we conclude that independent evidence exists for Na on the A site, association of Na with both Si as well as Al at the $T(1)$ sites, and the presence of some Al at the $M(3)$ in addition to the $M(2)$ sites, although the degree of disorder is unknown at present.

DISCUSSION

The development of composition-activity relations for chemically complex amphiboles has been a goal for decades, especially involving cation mixing derived from coexisting amphiboles (e.g., Powell 1975). Because magnesio-hornblende is an intermediate composition between the end-members tremolite and tschermakite, one can use constraints on the location of the miscibility gap between magnesio-hornblende and glaucophane provided in this study to refine the mixing properties of amphibole in the ternary system tremolite-glaucophane-tschermakite involving mixing of Ca and Na at the B, Al and Mg at the C, and Al and Si at the T crystallographic sites. Holland and Powell (2003) developed a means of modeling non-symmetric interactions for chemically complex phases, such as amphiboles, using a method referred to as asymmetric formalism (ASF). As discussed in detail by Dale et al. (2005), asymmetric mixing among the three components Gl, Tr, and Ts dealt with in this study requires six variables: three macroscopic interaction parameters ($W_{\text{Gl,Tr}}$, $W_{\text{Gl,Ts}}$, and $W_{\text{Tr,Ts}}$) and three size parameters (α_{Gl} , α_{Tr} , and α_{Ts}). Activities of individual components can be calculated as the product of the ideal activity (α_i^{ideal}) and the corresponding activity coefficient (γ_i). Ideal activities for Gl and Tr, the two components used here to model the miscibility gaps shown in the system $\text{Na}_2\text{O-CaO-MgO-Al}_2\text{O}_3\text{-SiO}_2\text{-H}_2\text{O}$, are

$$a_{\text{Gl}}^{\text{ideal}} = X_{\square}^{\text{A}} \left[X_{\text{Na}}^{\text{M4}} \right]^2 \left[X_{\text{Al}}^{\text{M2}} \right]^2 \left[X_{\text{Si}}^{\text{T1}} \right] \quad (3a)$$

$$a_{\text{Tr}}^{\text{ideal}} = X_{\square}^{\text{A}} \left[X_{\text{Ca}}^{\text{M4}} \right]^2 \left[X_{\text{Mg}}^{\text{M2}} \right]^2 \left[X_{\text{Si}}^{\text{T1}} \right] \quad (3b)$$

where X_i^j is the mole fraction of cation i on site j , the $M(1)$ and $M(3)$ sites are fully occupied by Mg, and \square is a vacancy. Note that the mole fraction on the tetrahedral $[T(1)]$ site is only raised to the first (rather than the fourth) power, as suggested by Dale et al. (2005), to minimize the magnitude of the activity coefficient for this component. The corresponding activity coefficient for the Gl and Tr components are then calculated for the ternary amphibole system tremolite-glaucophane-tschermakite as

$$\begin{aligned} RT \ln(\gamma_{\text{Gl}}) = & (1 - \phi_{\text{Gl}})(\phi_{\text{Tr}})W_{\text{Gl,Tr}} \left[\frac{2\alpha_{\text{Gl}}}{(\alpha_{\text{Gl}} + \alpha_{\text{Tr}})} \right] \\ & + (1 - \phi_{\text{Gl}})(\phi_{\text{Ts}})W_{\text{Gl,Ts}} \left[\frac{2\alpha_{\text{Gl}}}{(\alpha_{\text{Gl}} + \alpha_{\text{Ts}})} \right] \\ & - (\phi_{\text{Ts}})(\phi_{\text{Tr}})W_{\text{Tr,Ts}} \left[\frac{2\alpha_{\text{Gl}}}{(\alpha_{\text{Tr}} + \alpha_{\text{Ts}})} \right] \end{aligned} \quad (4a)$$

$$\begin{aligned} RT \ln(\gamma_{\text{Tr}}) = & (1 - \phi_{\text{Tr}})(\phi_{\text{Gl}})W_{\text{Gl,Tr}} \left[\frac{2\alpha_{\text{Tr}}}{(\alpha_{\text{Gl}} + \alpha_{\text{Tr}})} \right] \\ & + (1 - \phi_{\text{Tr}})(\phi_{\text{Ts}})W_{\text{Tr,Ts}} \left[\frac{2\alpha_{\text{Tr}}}{(\alpha_{\text{Tr}} + \alpha_{\text{Ts}})} \right] \\ & - (\phi_{\text{Ts}})(\phi_{\text{Gl}})W_{\text{Gl,Tr}} \left[\frac{2\alpha_{\text{Tr}}}{(\alpha_{\text{Gl}} + \alpha_{\text{Ts}})} \right] \end{aligned} \quad (4b)$$

where $\phi_i = (\alpha_i p_i) / (\alpha_{\text{Gl}} p_{\text{Gl}} + \alpha_{\text{Tr}} p_{\text{Tr}} + \alpha_{\text{Ts}} p_{\text{Ts}})$ and p_i is the mole fraction of component i . The activities of the Gl and Tr components are therefore the product of the ideal activity and activity coefficient, namely:

$$\alpha_{\text{Gl}} = \alpha_{\text{Gl}}^{\text{ideal}} \times \gamma_{\text{Gl}} \quad (5a)$$

$$\alpha_{\text{Tr}} = \alpha_{\text{Tr}}^{\text{ideal}} \times \gamma_{\text{Tr}} \quad (5b)$$

and the condition for equilibrium between coexisting Gl-rich and Tr-rich amphiboles can be expressed as

$$\alpha_{\text{Gl}}^{\text{glaucophane}} = \alpha_{\text{Gl}}^{\text{tremolite}} \quad (6)$$

$$\alpha_{\text{Tr}}^{\text{glaucophane}} = \alpha_{\text{Tr}}^{\text{tremolite}}$$

Values for the six parameters of interest were reported earlier by Diener and Powell (2012) based on natural two-amphibole assemblages; however, the experimental data given in this study on compositionally simpler amphiboles and with known values of P and T provide strong constraints on some of these parameters by avoiding the influence of other elements. Because only the relative values of α_i are important, it is customary to set one of the size parameters to unity, which is normally α_{Tr} (e.g., Diener et al. 2007). The values of $W_{\text{Gl,Tr}}$ and α_{Gl} were adopted from the study of Jenkins et al. (2014) as being 70 kJ and 0.52, respectively. The miscibility gap investigated in this study was considered to provide better constraints on $W_{\text{Gl,Ts}}$ than on $W_{\text{Tr,Ts}}$ because of the proximity of the miscibility gap to glaucophane (Figs. 7 and 13); therefore, the parameters $W_{\text{Gl,Ts}}$ and α_{Ts} were allowed to vary whereas the value of $W_{\text{Tr,Ts}}$ was taken from Diener and Powell (2012).

Values for the best-fit interaction and size parameters are listed in Table 9, with a set of isotherms through the ternary miscibility gap calculated using these parameters shown in Figure 13a; also shown are the compositions of amphiboles that limit the locations of these miscibility gaps. Data points along the tremolite-glaucophane join are from Jenkins et al. (2014), whereas data along the amphibole-“A”-glaucophane join are from this study. The points on the Tr- and Hb-rich side of the miscibility gaps lie noticeably off the gap because, as indicated above, these compositions probably indicate the absolute maximum width of the two-phase field at a given temperature because of sluggish re-equilibration kinetics. On the Gl-rich side of the miscibility gap the agreement is much better, with the highest-temperature data (700 °C) considered to have the closest approach to equilibrium and the corresponding closest fit. In addition to the limiting amphibole compositions, the cation mixing properties are strongly constrained by having the critical point lie below

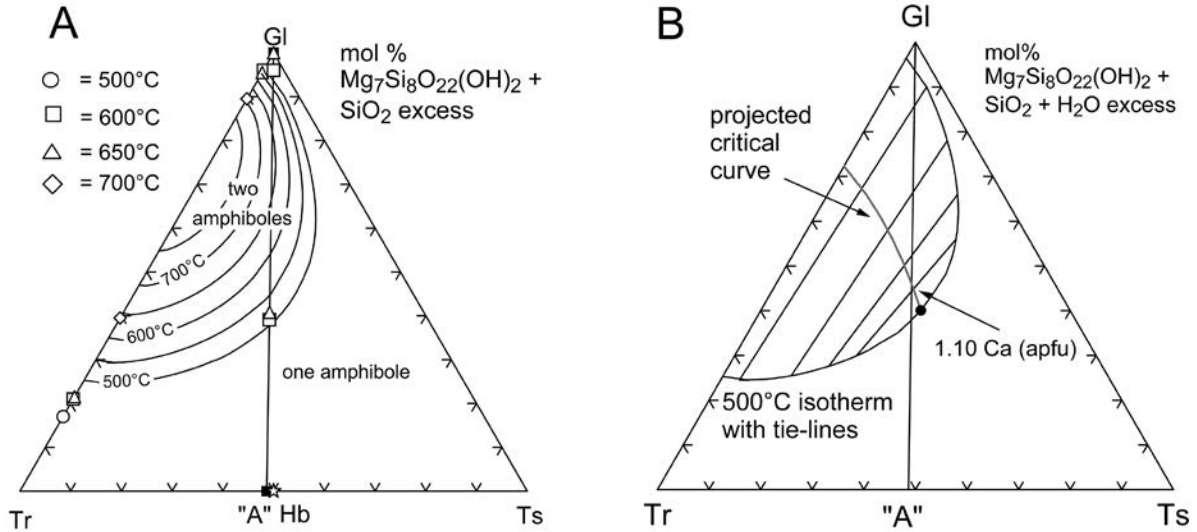


FIGURE 13. (a) Compositions of coexisting amphiboles along the join “A”-glaucophane from this study and along the join tremolite-glaucophane from the study of Jenkins et al. (2014). Legend indicates the temperatures of the coexisting amphiboles. Star is the composition of ideal magnesio-hornblende. Solid curves are calculated isotherms of the two-amphibole field as discussed in the text. (b) Calculated isothermal section at 500 °C showing the sense of the tie-lines.

700 °C for compositions along the amphibole-“A”-glaucophane join (Fig. 7). The shape of the solvus shown in Figure 7 can now be recognized as the intersection of the isotherms of the ternary miscibility gap with the “A”-Gl join. A fourth-order polynomial, namely $T(^{\circ}\text{C}) = 370.70 + 1535.32(\text{Ca}) - 2558.81(\text{Ca}^2) + 1653.95(\text{Ca}^3) - 411.53(\text{Ca}^4)$ where Ca is in atoms per formula unit (apfu), was used to model the solvus. This polynomial is provided only for the purpose of graphical representation and has no physical meaning.

Figure 13b shows a representative isothermal section with tie-lines connecting coexisting amphibole compositions. Note that the orientation of these tie-lines rotates toward the Ts corner as they converge at the critical-point composition (solid circle) on the miscibility gap. This behavior exists for any given isothermal section, and the critical points at any given temperature project as the gray curve shown on the figure. The compositional join “A”-Gl crosses the critical curve at a Ca content of 1.10 apfu. This composition corresponds to the maximum in the excess Gibbs free energy (G^{excess}) shown in Figure 14, where G^{excess} is calculated in ASF theory (Holland and Powell 2003) as:

$$G^{\text{excess}} = \phi_{\text{Gl}}\phi_{\text{Tr}}B_{\text{GlTr}} + \phi_{\text{Gl}}\phi_{\text{Ts}}B_{\text{GlTs}} + \phi_{\text{Tr}}\phi_{\text{Ts}}B_{\text{TrTs}} \quad (7)$$

where the values of ϕ_i are the same as defined previously and B_{ij} is calculated as $B_{ij} = 2\alpha_{ik}p_k/(\alpha_i + \alpha_j)$ with $k \neq i, j$.

We can now offer some explanation for the contradiction between the sense of miscibility-gap asymmetry indicated by the autocorrelation results shown in Figure 11 and its shape in Figure 7. Realizing that the join investigated in this study is a section through the ternary system tremolite-glaucophane-tschermakite, the tie-lines join amphiboles whose compositions lie outside of the bounds of this pseudo-binary section, not within the section, and converge to critical points that are relatively Ca-rich. For the two frequency ranges that yielded a clear autocorrelation signal,

TABLE 9. Macroscopic interaction parameters (W_i) and size parameters (α_i) from this study and that of Diener and Powell (2012)

Parameter	This study	Diener and Powell (2012)
$W_{\text{Gl,Tr}}$, kJ	70 ^a	65
$W_{\text{Gl,Ts}}$, kJ	20	25
$W_{\text{Tr,Ts}}$, kJ	20	20
α_{Gl}	0.52 ^a	0.8
α_{Tr}	1.0	1.0
α_{Ts}	1.2	1.5

^aValues based on the tremolite-glaucophane join (Jenkins et al. 2014).

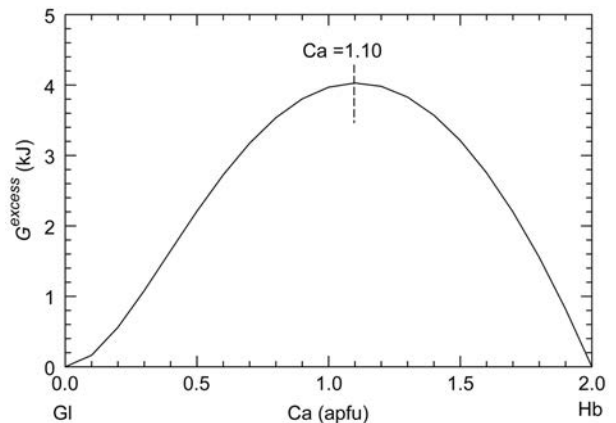


FIGURE 14. Calculated excess Gibbs free energy (G^{excess}) along the magnesio-hornblende-glaucophane join using the size parameters (α_i) and macroscopic interaction parameters (W_{ij}) from this study (Table 9) and Equation 7.

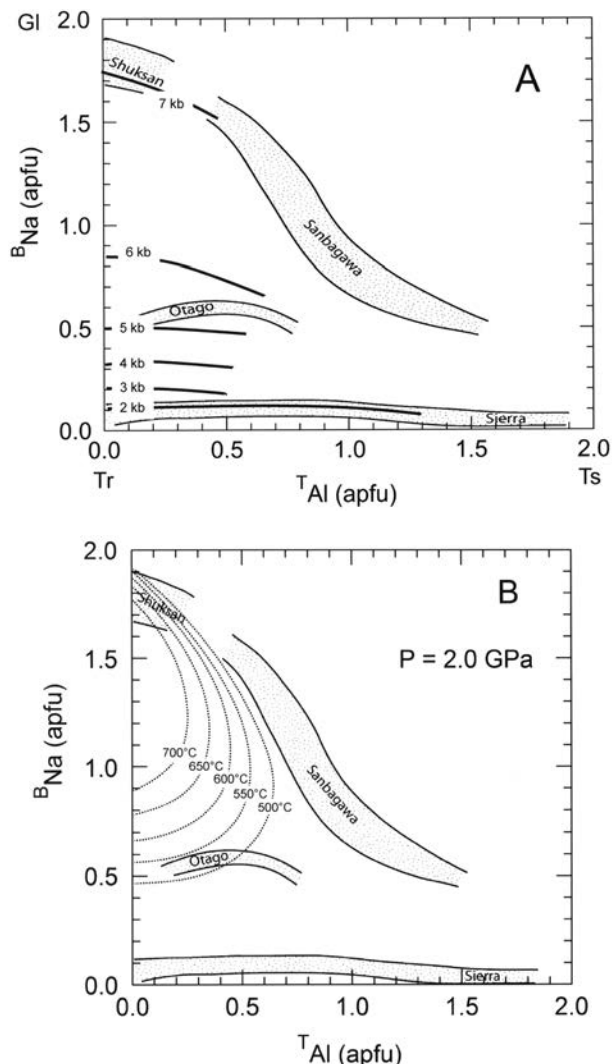


FIGURE 15. (a) Figure showing the correlation between B_{Na} and T_{Al} for amphiboles coexisting with albite, chlorite, and iron oxide after Figure 10 of Brown (1977). Locality abbreviations are: Shuksan = northern Cascades, Washington; Sanbagawa = Sanbagawa terrane, central Shikoku, Japan; Otago = metamorphic terrane of western Otago, south island, New Zealand; and Sierra = contact aureoles of Sierra Nevada, California. (b) Isotherms of the miscibility gap shown in Figure 13a superimposed on the compositional plot of Brown (1977). Note the close agreement between the amphibole compositions and the location of the miscibility gap, particularly at the lower-temperature range, suggesting that temperature, rather than pressure, has the dominant control on amphibole compositions.

namely the 162–224 cm^{-1} (“200” cm^{-1}) and 620–1300 cm^{-1} (“800” cm^{-1}) ranges, the maximum values of $\delta\Delta_{\text{Corr}}$ are in the Ca ranges of 1.15–1.4 and 0.9–1.38 apfu, respectively, which are relatively close to the maximum of 1.10 apfu in the G^{excess} curve of Figure 14. We stress that placement of the isotherms in Figure 13a was based solely on the composition–temperature constraints (Figs. 5 and 7) on the location of the miscibility gap along the tremolite–glaucophane and magnesio-hornblende–glaucophane joins and was done independently of the autocorrelation results in Figure 11.

IMPLICATIONS

The magnesio-hornblende–glaucophane join studied here along with the thermodynamic modeling of the two-amphibole region in the tremolite–glaucophane–tschermakite ternary system provide important insights into the compositional variations observed for sodium- and calcium-sodium-amphiboles in nature. Brown (1977) compiled amphibole compositions from various metamorphic terranes where the amphibole compositions were buffered by coexisting albite, chlorite, and iron oxide. The resultant “geo-experimental” diagram (cf. Newton 2011), reproduced as Figure 15a here, shows systematic variations in the Na content of the $M(4)$ site with Al at the $T(1)$ site, so long as the amphiboles occur in equilibrium with the buffering minerals. These variations were considered to be controlled primarily by pressure. Although Brown (1977) noted that a miscibility gap might exist between calcium- and sodium-amphiboles at high P , he proposed that there was complete miscibility at the greenschist or lower-pressure portion of the blueschist facies. Figure 15a from Brown (1977), being both an elegant and simple use of calcium-amphibole chemical variations to deduce P , has been cited often since its publication, with an average yearly citation of ~200 (Web of Science 2014).

The ternary system tremolite–glaucophane–tschermakite comprises essentially all of the amphibole compositions shown in Figure 15a, so that the results from this study should have some relevance to this diagram. Figure 15b has the isotherms from Figure 13a superimposed on it. The amphibole compositions from the Otago, Shuksan, and Sanbagawa terranes agree closely with the isotherms at 500–550 °C. Although Brown (1977) discounted the role of amphibole immiscibility in this diagram, the striking agreement between the amphibole compositions observed in nature and the lower-temperature portion of the miscibility gap determined in this study suggests immiscibility may be more important than pressure. Since the study of Brown (1977), evidence has been presented for coexisting sodium- and calcium-amphiboles in low-grade metabasaltic rocks from various blueschist-facies terranes (e.g., Ernst 1979). Further improvements in quantifying the conditions under which calcium-rich and sodium-rich amphiboles form in the presence of the buffering mineral assemblage can be obtained by extending the mixing properties of amphiboles to include ferrous- and ferric-iron components. Preliminary results of amphibole compositions coexisting with chlorite, plagioclase, and epidote in a model mid-ocean-ridge basalt bulk composition using the parameters derived from this study, with the parameters for other amphibole components (e.g., Diener and Powell 2012), were presented by Jenkins and Lei (2013) and will be the subject of a more detailed publication.

ACKNOWLEDGMENTS

Financial support for this study was provided by NSF grant EAR-0947175 to D.M.J. We thank David Collins for his help with the electron microprobe analyses. The manuscript was greatly improved by the thorough reviews of W.G. Ernst and G. Lezzi.

REFERENCES CITED

- Atkinson, A.J., Carpenter, M.A., and Salje, E.K.H. (1999) Hard-mode infrared spectroscopy of plagioclase feldspars. *European Journal of Mineralogy*, 11, 7–21.
- Basora, A.M., Jenkins, D.M., and Bish, D.L. (2012) The lower-pressure stability of glaucophane in the presence of paragonite and quartz in the system Na_2O –

- MgO-Al₂O₃-SiO₂-H₂O. *American Mineralogist*, 97, 713–726.
- Benisek, A., Dachs, E., and Kroll, H. (2014) Thermochemistry of the alkali feldspars: Calorimetric study of the entropy relations in the low albite–low microcline series. *American Mineralogist*, 99, 76–83.
- Bish, D.L., and Post, J.E. (1993) Quantitative mineralogical analysis using the Rietveld full-pattern fitting method. *American Mineralogist*, 78, 932–940.
- Boffa Ballaran, T., and Carpenter, M.A. (2003) Line broadening and enthalpy: some empirical calibrations of solid solution behaviour from IR spectra. *Phase Transitions*, 76, 137–154.
- Boffa Ballaran, T., Carpenter, M.A., Domeneghetti, M.C., Salje, E.K.H., and Tazzoli, V. (1998) Structural mechanism of solid solution and cation ordering in augite–jadeite pyroxenes II: a microscopic perspective. *American Mineralogist*, 83, 419–433.
- Boffa Ballaran, T., Carpenter, M.A., Geiger, C.A., and Koziol, A.M. (1999) Local structural heterogeneity in garnet solid solutions. *Physics and Chemistry of Minerals*, 26, 554–569.
- Boffa Ballaran, T., Carpenter, M.A., and Domeneghetti, M.C. (2001) Phase transition and mixing behaviour of the cummingtonite–grunerite solid solution. *Physics and Chemistry of Minerals*, 28, 87–101.
- Bozhilov, K.N., Brownstein, D., and Jenkins, D.M. (2007) Biopyribole evolution during tremolite synthesis from dolomite and quartz in CO₂-H₂O fluid. *American Mineralogist*, 92, 898–908.
- Brown, E.H. (1977) The crossite content of Ca-amphibole as a guide to pressure of metamorphism. *Journal of Petrology*, 18, 53–72.
- Cao, R.L., Ross, C., and Ernst, W.G. (1986) Experimental studies to 10 kb of the bulk composition tremolite₅₀-tschermakite₅₀ + excess H₂O. *Contributions to Mineralogy and Petrology*, 93, 160–167.
- Carpenter, M.A. (2002) Microscopic strain, macroscopic strain and the thermodynamics of phase transitions in minerals. In C.M. Gramaccioli, Ed., *Energy Modelling in Minerals*, European Mineralogical Union Notes in Mineralogy, 4, 311–346.
- Carpenter, M.A., and Boffa Ballaran, T. (2001) The influence of elastic strain heterogeneities in silicate solid solutions. In C.A. Geiger, Ed., *Solid Solutions in Silicate and Oxide Systems*, European Mineralogical Union Notes in Mineralogy, 3, 155–178.
- Cho, M., and Ernst, W.G. (1991) An experimental determination of calcic amphibole solid solution along the join tremolite-tschermakite. *American Mineralogist*, 76, 985–1001.
- Corona, J.C., and Jenkins, D.M. (2007) An experimental investigation of the reaction: glaucophane + 2 quartz = 2 albite + talc. *European Journal of Mineralogy*, 19, 147–158.
- Corona, J.C., Jenkins, D.M., and Holland, T.J.B. (2013) Constraints on the upper pressure stability of blueschist facies metamorphism along the reaction: glaucophane = talc + 2 jadeite in the Na₂O-MgO-Al₂O₃-SiO₂-H₂O system. *American Journal of Science*, 313, 967–995.
- Davies, P.K., and Navrotsky, A. (1983) Quantitative correlations of deviations from ideality in binary and pseudobinary solid solutions. *Journal of Solid State Chemistry*, 46, 1–22.
- Dale, J., Powell, R., White, R.W., Elmer, F.L., and Holland, T.J.B. (2005) A thermodynamic model for Ca-Na clinooamphiboles in Na₂O-CaO-FeO-MgO-Al₂O₃-SiO₂-H₂O-O for petrological calculations. *Journal of Metamorphic Geology*, 23, 771–791.
- Della Ventura, G., Hawthorne, F.C., Robert, J.-L., Delbove, F., Welch, M.D., and Raudsepp, M. (1999) Short-range order of cations in synthetic amphiboles along the richterite-pargasite join. *European Journal of Mineralogy*, 11, 79–94.
- Della Ventura, G., Hawthorne, F.C., Robert, J.-L., and Iezzi, G. (2003) Synthesis and infrared spectroscopy of amphiboles along the tremolite-pargasite join. *European Journal of Mineralogy*, 15, 341–347.
- Diener, J.F.A., and Powell, R. (2012) Revised activity-composition models for clinopyroxene and amphibole. *Journal of Metamorphic Geology*, 30, 131–142.
- Diener, J.F.A., Powell, R., White, R.W., and Holland, T.J.B. (2007) A new thermodynamic model for clino-orthoamphiboles in the system Na₂O-CaO-FeO-MgO-Al₂O₃-SiO₂-H₂O-O. *Journal of Metamorphic Geology*, 25, 631–656.
- Ernst, W.G. (1963) Petrogenesis of glaucophane schists. *Journal of Petrology*, 4, 1–30.
- (1979) Coexisting sodic and calcic amphiboles from relatively high pressure metamorphic belts and the stability of barroisitic amphibole. *Mineralogical Magazine*, 43, 269–278.
- Etzel, K., and Benisek, A. (2008) thermodynamic mixing behavior of synthetic Ca-Tschermak-diopside pyroxene solid solutions: III. An analysis of IR line broadening and heat of mixing behavior. *Physics and Chemistry of Minerals*, 35, 399–407.
- Evans, B.W., Ghiorsio, M.S., and Kuehner, S.K. (2000) Thermodynamic properties of tremolite: A correction and some comments. *American Mineralogist*, 85, 466–472.
- Gottschalk, M., Andrut, M., and Melzer, S. (1999) The determination of the cummingtonite content of synthetic tremolite. *European Journal of Mineralogy*, 11, 967–982.
- Graham, C.M., Maresch, W.V., Welch, M.D., and Pawley, A.R. (1989) Experimental studies on amphiboles: A review with thermodynamic perspectives. *European Journal of Mineralogy*, 1, 535–555.
- Hammarstrom, J.M., and Zen, E. (1986) Aluminum in hornblende—An empirical igneous geobarometer. *American Mineralogist*, 71, 1297–1313.
- Hawthorne, F.C., and Della Ventura, G. (2007) Short-range order in amphiboles. *Reviews in Mineralogy and Geochemistry*, 67, 173–222.
- Hawthorne, F.C., and Oberti, R. (2007) Amphiboles: Crystal chemistry. *Reviews in Mineralogy and Geochemistry*, 67, 1–54.
- Hawthorne, F.C., Welch, M.D., Della Ventura, G., Liu, S., Robert, J.-L., and Jenkins, D.M. (2000) Short-range order in synthetic aluminous tremolite: An infrared and triple-quantum MAS NMR study. *American Mineralogist*, 85, 1716–1724.
- Hill, R.J., and Flack, H.D. (1987) The use of the Durbin-Watson *d* statistic in Rietveld analysis. *Journal of Applied Crystallography*, 20, 356–361.
- Himmelberg, G.R., and Papike, J.J. (1969) Coexisting amphiboles from blueschist facies metamorphic rocks. *Journal of Petrology*, 10, 102–114.
- Hirschmann, M., Evans, B.W., and Yang, H. (1994) Composition and temperature dependence of Fe-Mg ordering in cummingtonite-grunerite as determined by X-ray diffraction. *American Mineralogist*, 79, 862–877.
- Holland, T., and Blundy, J. (1994) Non-ideal interactions in calcic amphiboles and their bearing on amphibole-plagioclase thermometry. *Contributions to Mineralogy and Petrology*, 116, 433–447.
- (2003) Activity-composition relations for phases in petrological calculations: an asymmetric multicomponent formulation. *Contributions to Mineralogy and Petrology*, 145, 492–501.
- Hoschek, G. (1995) Stability relations and Al content of tremolite and talc in CMASH assemblages with kyanite + zoisite + quartz + H₂O. *European Journal of Mineralogy*, 7, 353–362.
- Iezzi, G., Della Ventura, G., Tribaudino, M., Nemeth, P., Margiolaki, I., Cavallo, A., Gaillard, F., and Behrens, H. (2010) Phase transition induced by solid solution: The ⁸Ca-⁹Mg substitution in richteritic amphiboles. *American Mineralogist*, 95, 369–381.
- Jasmund, K., and Schäfer, R. (1972) Experimentelle Bestimmung der P-T-Stabilitätsbereiche in der Mishkristallreihe Tremolite-Tschermakite. *Contributions to Mineralogy and Petrology*, 34, 101–115.
- Jenkins, D.M. (1987) Synthesis and characterization of tremolite in the system H₂O-CaO-MgO-SiO₂. *American Mineralogist*, 72, 707–715.
- (1988) Experimental study of the join tremolite-tschermakite: A reinvestigation. *Contributions to Mineralogy and Petrology*, 99, 392–400.
- (1994) Experimental reversal of the aluminum content in tremolitic amphiboles in the system H₂O-CaO-MgO-Al₂O₃-SiO₂. *American Journal of Science*, 294, 593–620.
- (2011) The transition from blueschist to greenschist facies modeled by the reaction glaucophane + 2 diopside + 2 quartz = tremolite + 2 albite. *Contributions to Mineralogy and Petrology*, 162, 725–738.
- Jenkins, D.M., and Clare, A.K. (1990) Comparison of the high-temperature and high-pressure stability limits of synthetic and natural tremolite. *American Mineralogist*, 75, 358–366.
- Jenkins, D.M., and Corona, J.C. (2006a) The role of water in the synthesis of glaucophane. *American Mineralogist*, 91, 1055–1068.
- (2006b) Molar volume and thermal expansion of glaucophane. *Physics and Chemistry of Minerals*, 33, 356–362.
- Jenkins, D.M., and Lei, J. (2013) Pressure and temperature variation of octahedral Na and tetrahedral Al in amphiboles in metamorphic rocks. *American Geophysical Union, Fall Meeting, San Francisco, Abstract V13C-2630*.
- Jenkins, D.M., Della Ventura, G., Oberti, R., and Bozhilov, K. (2013) Synthesis and characterization of amphiboles along the tremolite-glaucophane join. *American Mineralogist*, 98, 588–600.
- Jenkins, D.M., Carpenter, M.A., and Zhang, M. (2014) Experimental and infrared characterization of the miscibility gap along the tremolite-glaucophane join. *American Mineralogist*, 99, 730–741.
- Larson, A.C., and Von Dreele, R.B. (2000) General Structure Analysis System (GSAS). Los Alamos National Laboratory Report LAUR 86-748.
- Levien, L., Prewitt, C.T., and Weidner, D.J. (1980) Structure and elastic properties of quartz at pressure. *American Mineralogist*, 65, 920–930.
- Lindsley, D.H., and Dixon, S.A. (1976) Diopside-enstatite equilibria at 850° to 1400°C, 5 to 35 kb. *American Journal of Science*, 276, 1285–1301.
- Liou, J.G., Maruyama, S., and Cho, M. (1985) Phase equilibria and mineral parageneses of metabasites in low-grade metamorphism. *Mineralogical Magazine*, 49, 321–333.
- Maresch, W.V., Medenbach, O., and Rudolph, A. (1982) Winchite and the actinolite-glaucophane miscibility gap. *Nature*, 296, 731–732.
- Maresch, W.V., Czank, M., and Schreyer, W. (1994) Growth mechanism, structural defects and composition of synthetic tremolite: What are the effects on macroscopic properties? *Contributions to Mineralogy and Petrology*, 118, 297–313.
- Maruyama, S., Cho, M., and Liou, J. (1986) Experimental investigations of blueschist-greenschist transition equilibria: Pressure dependence of Al₂O₃ contents in sodic amphiboles—A new geobarometer. In B.W. Evans and E.H. Brown, Eds., *Blueschists and Eclogites*, Geological Society of America, Memoir 164, 1–16.

- Maruyama, S., Liou, J.G., and Terabayashi, M. (1996) Blueschists and eclogites of the world and their exhumation. *International Geology Review*, 38, 485–594.
- Najorka, J., and Gottschalk, M. (2003) Crystal chemistry of tremolite-tschermakite solid solutions. *Physics and Chemistry of Minerals*, 30, 108–124.
- Newton, R.C. (2011) The three partners of metamorphic petrology. *American Mineralogist*, 96, 457–469.
- Oberti, R., Hawthorne, F.C., Ungaretti, L., and Cannillo, E. (1995) ⁶⁷Al disorder in amphiboles from mantle peridotites. *Canadian Mineralogist*, 33, 867–878.
- Palin, E.J., Guiton, B.S., Craig, M.S., Welch, M.D., Dove, M.T., and Redfern, S.A.T. (2003) Computer simulation of Al-Mg ordering in glaucophane and a comparison with infrared spectroscopy. *European Journal of Mineralogy*, 15, 893–901.
- Papike, J.J., and Clark, J.R. (1968) The crystal structure and cation distribution of glaucophane. *American Mineralogist*, 53, 1156–1173.
- Pawley, A.R. (1992) Experimental study of the compositions and stabilities of synthetic nyböite and nyböite-glaucophane amphiboles. *European Journal of Mineralogy*, 4, 171–192.
- Perdikatsis, B., and Burzlaff, H. (1981) Strukturverfeinerung am Talk Mg₃[(OH)₂Si₄O₁₀]. *Zeitschrift für Kristallographie*, 156, 177–186.
- Powell, R. (1975) Thermodynamics of coexisting cummingtonite-hornblende pairs. *Contributions to Mineralogy and Petrology*, 51, 29–37.
- Reynard, B., and Ballèvre, M. (1988) Coexisting amphiboles in an eclogite from the Western Alps: new constraints on the miscibility gap between sodic and calcic amphiboles. *Journal of Metamorphic Geology*, 6, 333–350.
- Salje, E.K.H., Carpenter, M.A., Malcherek, T.G.W., and Boffa Ballaran, T. (2000) Autocorrelation analysis of infrared spectra. *European Journal of Mineralogy*, 12, 503–519.
- Schmidt, M.W. (1992) Amphibole composition in tonalite as a function of pressure—An experimental calibration of the Al-in-hornblende barometer. *Contributions to Mineralogy and Petrology*, 110, 304–310.
- Schumacher, J.C. (2007) Metamorphic amphiboles: Composition and coexistence. *Reviews in Mineralogy and Geochemistry*, 67, 359–416.
- Sharma, A., and Jenkins, D.M. (1999) Hydrothermal synthesis of amphiboles along the tremolite-pargasite join and in the ternary system tremolite-pargasite-cummingtonite. *American Mineralogist*, 84, 1304–1318.
- Shirozu, H., and Bailey, S.W. (1966) Crystal structure of a two-layer Mg-vermiculite. *American Mineralogist*, 51, 1124–1143.
- Smelik, E.A., and Veblen, D.R. (1992) Exsolution of Ca-amphibole from glaucophane and the miscibility gap between sodic and calcic amphiboles. *Contributions to Mineralogy and Petrology*, 112, 178–195.
- Tarantino, S.C., Boffa Ballaran, T., Carpenter, M.A., Domeneghetti, M.A., and Tazzoli, V. (2002) Mixing properties of the enstatite-ferrosilite solid solution: II. A microscopic perspective. *European Journal of Mineralogy*, 14, 537–547.
- Vernon, R.H., and Clarke, G. (2008) *Principles of Metamorphic Petrology*, 446 pp. Cambridge University Press, New York.
- Walker, D., Verma, P.K., Cranswick, L.M.D., Clark, S.M., Jones, R.L., and Buhre, S. (2005) Halite-sylvite thermoconsolution. *American Mineralogist*, 90, 229–239.
- Web of Science. (2014) Thomson Reuters, Accessed April, 14, 2014.
- Welch, M.D., and Pawley, A.R. (1991) Tremolite: new enthalpy and entropy data from a phase equilibrium study of the reaction tremolite = 2 diopside + 1.5 orthoenstatite + β-quartz + H₂O. *American Mineralogist*, 76, 1931–1939.
- Zimmermann, R., Heinrich, W., and Franz, G. (1996) Tremolite synthesis from CaCl₂-bearing aqueous solutions. *European Journal of Mineralogy*, 8, 767–776.

MANUSCRIPT RECEIVED APRIL 29, 2014

MANUSCRIPT ACCEPTED AUGUST 25, 2014

MANUSCRIPT HANDLED BY EDWARD GHENT